

Robust Multilinear Principal Component Analysis

Mehdi Hirari¹, Fabio Centofanti^{1,2}, Mia Hubert^{*1}, and Stefan Van Aelst¹

¹Section of Statistics and Data Science, Department of Mathematics, KU Leuven, Belgium

²Department of Industrial Engineering, University of Naples Federico II, Naples, Italy

March 10, 2025

Abstract

Multilinear Principal Component Analysis (MPCA) is an important tool for analyzing tensor data. It performs dimension reduction similar to PCA for multivariate data. However, standard MPCA is sensitive to outliers. It is highly influenced by observations deviating from the bulk of the data, called casewise outliers, as well as by individual outlying cells in the tensors, so-called cellwise outliers. This latter type of outlier is highly likely to occur in tensor data, as tensors typically consist of many cells. This paper introduces a novel robust MPCA method that can handle both types of outliers simultaneously, and can cope with missing values as well. This method uses a single loss function to reduce the influence of both casewise and cellwise outliers. The solution that minimizes this loss function is computed using an iteratively reweighted least squares algorithm with a robust initialization. Graphical diagnostic tools are also proposed to identify the different types of outliers that have been found by the new robust MPCA method. The performance of the method and associated graphical displays is assessed through simulations and illustrated on two real datasets.

Keywords: Anomaly detection; Casewise outliers; Cellwise outliers; Multiway data; Robust statistics; Tensor data.

*Corresponding author. e-mail: Mia.Hubert@kuleuven.be

1 Introduction

In many real-world scenarios, data are naturally represented as tensors, i.e., multiway arrays where each dimension or mode encodes specific characteristics of the data objects. For example, video data consist of a sequence of frames where each frame can be represented by a three-dimensional tensor where the first two modes characterize pixel location and the third mode is a color encoding of each pixel. See the Dog Walker video data in Section 5.1 for an example.

A common practice to analyze such data is to reshape or vectorize it so that matrix-based models and methods can be applied. However, this approach often breaks the natural structure and correlations of the data, removing higher-order dependencies, for instance. This can lead to the loss of more compact and meaningful representations that could be preserved in the original multidimensional form (Ye et al., 2004). On the other hand, tensor-based multilinear data analysis has shown that tensor models can effectively leverage the multilinear structure of the data, providing better insights and precision. An important aspect of multilinear data analysis is tensor decomposition, typically performed using either a CANDECOMP/PARAFAC (CP) decomposition (Carroll and Chang, 1970; Harshman, 1970) or a Tucker decomposition (Tucker, 1966). Originally developed in the fields of psychometrics and chemometrics (Smilde et al., 2004; Kroonenberg, 2008), these decomposition techniques have gained visibility in various areas, including computer vision (Vasilescu and Terzopoulos, 2007; Zhao et al., 2015; Shi et al., 2018), medical imaging (Goldfarb and Qin, 2014; Liu et al., 2015), and signal processing (De Lathauwer et al., 2000).

Lu et al. (2008) introduced a new method for tensor decomposition, Multilinear Principal Component Analysis (MPCA), with an application in gait recognition (Han and Bhanu, 2005; Sarkar et al., 2005). MPCA extends the classical PCA paradigm and performs dimensionality reduction across all tensor modes by identifying a basis for each mode such that the projected tensors capture the maximum amount of variation present in the data.

As for other data types, also for tensor data a common issue that may arise is the presence of outliers. Robust methods address this issue by constructing fits that are little affected by outliers. These robust methods then make it possible to identify outliers based on their deviation from the robust fit. Since its inception in the 1960s, research in robust statistics mainly focused on casewise outliers, which is the setting where a minority of entire observations can deviate from the bulk of the data. However, the advent of high-dimensional data instigated a paradigm shift in robust statistics towards cellwise outliers (Alqallaf et al., 2009), where the focus is on individual cells that deviate from the bulk of the data. Cellwise robust methods on the one hand aim to mitigate the effect of the deviating cells while on the other hand they want to preserve the valuable information in the other components of these observations. Ideally, modern robust methods can handle both cellwise and casewise outliers. Another common issue usually encountered in practice is the presence of missing entries, so a versatile method should be able to handle missing data as

well.

In the multivariate setting, it is well-known that classical PCA is not robust. Several methods have been developed that are robust in the presence of casewise outliers (Locantore et al., 1999; Croux and Ruiz-Gazen, 2005; Hubert et al., 2005). Serneels and Verdonck (2008) proposed a case-wise robust PCA method that can also cope with missing data. De La Torre and Black (2003) and Maronna and Yohai (2008) proposed robust methods for data containing cellwise outliers and missing values. The more recently proposed MacroPCA (Hubert et al., 2019) and cellPCA (Centofanti et al., 2024) methods can handle missing values, cellwise and casewise outliers simultaneously.

Similarly to PCA, the standard PARAFAC, Tucker and MPCA methods for tensor decomposition are sensitive to both casewise and cellwise outliers. Robust methods for PARAFAC decomposition include the casewise robust method of Engelen and Hubert (2011) and Todorov et al. (2023), its extension for tensors with missing data Hubert et al. (2012) and the MacroPARAFAC method (Hubert and Hirari, 2024) that can handle cellwise outliers as well. Inoue et al. (2009) introduced robust adaptations of MPCA that can either deal with casewise or cellwise outliers in the data. However, there does not yet exist an MPCA method that can simultaneously handle both types of outliers as well as missing values.

We introduce a robust MPCA method (ROMPCA) capable of managing both types of outliers and missing values. ROMPCA minimizes a single loss function in which the effect of both casewise and cellwise outliers is appropriately dampened, while missing cells are discarded to avoid the need for a robust imputation strategy. Section 2 introduces basic multilinear concepts and our newly proposed ROMPCA method. To solve the ROMPCA minimization problem, we introduce an iteratively reweighted least squares algorithm which uses alternating least squares in each iteration step. Section 3 evaluates its performance through extensive simulations while Section 4 presents several diagnostics to detect and visualize outlying cells and cases. Finally, we apply our method to two real datasets in Section 5 and Section 6 concludes.

2 Methodology

2.1 Preliminaries and Notation

This section reviews some of the basic multilinear concepts and notations that will be used throughout the paper. More details can be found in Lu et al. (2008). An L -order tensor is denoted as $\mathcal{A} = [a_{p_1 \dots p_L}] \in \mathbb{R}^{P_1 \times \dots \times P_L}$ where each of the L indices $p_\ell = 1, \dots, P_\ell$ addresses the mode- ℓ of \mathcal{A} . The tensor \mathcal{A} resides in the tensor space $\mathbb{R}^{P_1} \otimes \dots \otimes \mathbb{R}^{P_L}$, which is the tensor product (outer product) of L vector spaces $\mathbb{R}^{P_1}, \dots, \mathbb{R}^{P_L}$. The mode- ℓ vectors of \mathcal{A} are defined as the P_ℓ -dimensional vectors obtained from \mathcal{A} by varying the index p_ℓ while keeping all the other indices fixed. For instance, $\mathcal{A}_{:,p_2,\dots,p_L}$ is a mode-1 vector, where the colon notation $:$ indicates the full range of a given index.

The p_ℓ th mode- ℓ slice of \mathcal{A} is obtained by fixing the mode- ℓ index of \mathcal{A} to be p_ℓ , i.e., $\mathcal{A}_{\dots, p_\ell, \dots}$. The mode- ℓ unfolding of \mathcal{A} is denoted as $\mathbf{A}_{(\ell)} \in \mathbb{R}^{P_\ell \times (P_1 \cdots P_{\ell-1} P_{\ell+1} \cdots P_L)}$ whose column vectors are the mode- ℓ vectors of \mathcal{A} . The order of the columns of the mode- ℓ vectors in $\mathbf{A}_{(\ell)}$ is not important as long as it is consistent throughout the computation. The operation $\text{vec}(\mathcal{A})$ vectorizes any tensor \mathcal{A} into a column vector $\mathbf{a} \in \mathbb{R}^{\prod_{\ell=1}^L P_\ell}$.

The mode- ℓ product of a tensor \mathcal{A} by a matrix $\mathbf{V} = [v_{p_\ell k_\ell}] \in \mathbb{R}^{P_\ell \times K_\ell}$ is a tensor $\mathcal{B} = [b_{p_1 \dots p_L}] \in \mathbb{R}^{P_1 \times \dots \times P_{\ell-1} \times K_\ell \times P_{\ell+1} \times \dots \times P_L}$, denoted by $\mathcal{B} = \mathcal{A} \times_\ell \mathbf{V}^T$, where each entry of \mathcal{B} is defined as the sum of products of corresponding entries in \mathcal{A} and \mathbf{V} , that is $b_{p_1 \dots p_{\ell-1} k_\ell p_{\ell+1} \dots p_L} = \sum_{p_\ell=1}^{P_\ell} a_{p_1 \dots p_L} v_{p_\ell k_\ell}$.

Any L -order tensor \mathcal{A} can be decomposed as the mode- ℓ product of an L -order core tensor \mathcal{B} and a collection of L matrices $\mathbf{V}^{(\ell)} \in \mathbb{R}^{P_\ell \times P_\ell}$ with orthonormal columns, as follows

$$\mathcal{A} = \mathcal{B} \times_1 \mathbf{V}^{(1)} \times_2 \cdots \times_L \mathbf{V}^{(L)} := \mathcal{B} \times \{\mathbf{V}\}, \quad (1)$$

where $\mathcal{B} = \mathcal{A} \times_1 \mathbf{V}^{(1)T} \times_2 \cdots \times_L \mathbf{V}^{(L)T} := \mathcal{A} \times \{\mathbf{V}^T\}$ (Tucker, 1966). This decomposition can also be expressed using either vector or matrix formulation (Kolda, 2006) as follows

$$\begin{aligned} \text{vec}(\mathcal{A}) &= (\mathbf{V}^{(L)} \otimes \cdots \otimes \mathbf{V}^{(1)}) \text{vec}(\mathcal{B}) := \left(\bigotimes_{\ell=1}^L \mathbf{V}^{(\ell)} \right) \text{vec}(\mathcal{B}), \\ \mathbf{A}_{(\ell)} &= \mathbf{V}^{(\ell)} \mathbf{B}_{(\ell)} (\mathbf{V}^{(L)} \otimes \cdots \otimes \mathbf{V}^{(\ell+1)} \otimes \mathbf{V}^{(\ell-1)} \otimes \cdots \otimes \mathbf{V}^{(1)})^T, \end{aligned}$$

where \otimes denotes the Kronecker product. The mode- ℓ product of \mathcal{A} over *all but one* of the collection of matrices $\mathbf{V}^{(\ell)}$ is defined as

$$\mathcal{A}^{(-\ell)} = \mathcal{A} \times_1 \mathbf{V}^{(1)T} \times_2 \cdots \times_{\ell-1} \mathbf{V}^{(\ell-1)T} \times_{\ell+1} \mathbf{V}^{(\ell+1)T} \times_{\ell+2} \cdots \times_L \mathbf{V}^{(L)T} := \mathcal{A} \times_{-\ell} \{\mathbf{V}^T\}.$$

The inner product between two tensors of the same dimension \mathcal{A} and \mathcal{B} is defined as

$$\langle \mathcal{A}, \mathcal{B} \rangle = \sum_{p_1=1}^{P_1} \sum_{p_2=1}^{P_2} \cdots \sum_{p_L=1}^{P_L} a_{p_1 \dots p_L} b_{p_1 \dots p_L} := \sum_{p_1 \dots p_L}^{P_1 \dots P_L} a_{p_1 \dots p_L} b_{p_1 \dots p_L},$$

and the Frobenius norm of a tensor is $\|\mathcal{A}\|_F = \sqrt{\langle \mathcal{A}, \mathcal{A} \rangle}$.

The contracted product of the tensors $\mathcal{A} = [a_{p_1 \dots p_L j_1 \dots j_M}] \in \mathbb{R}^{P_1 \times \dots \times P_L \times J_1 \times \dots \times J_M}$ and $\mathcal{B} = [b_{p_1 \dots p_L k_1, \dots, k_N}] \in \mathbb{R}^{P_1 \times \dots \times P_L \times K_1 \times \dots \times K_N}$ along the first L modes is a tensor $\mathcal{D} = \langle \mathcal{A}, \mathcal{B} \rangle_{\{J_1, \dots, J_M; K_1, \dots, K_N\}} = [d_{j_1 \dots j_M k_1 \dots k_N}] \in \mathbb{R}^{J_1 \times \dots \times J_M \times K_1 \times \dots \times K_N}$ with $d_{j_1 \dots j_M k_1 \dots k_N} = \sum_{p_1 \dots p_L}^{P_1 \dots P_L} a_{p_1 \dots p_L j_1 \dots j_M} b_{p_1 \dots p_L k_1, \dots, k_N}$.

The identity matrix of dimension P_ℓ is denoted by \mathbf{I}_{P_ℓ} . A zero tensor and zero matrix are denoted by $\mathcal{O}_{P_1 \times \dots \times P_L}$ and $\mathbf{0}_{P_\ell \times K_\ell}$, where the subscripts indicate their dimensions.

2.2 Multilinear Principal Component Analysis

Let $\{\mathcal{X}_n = [x_{n, p_1 \dots p_L}]\}_{n=1}^N$ be a given set of N independent L -order tensors. The objective of tensor dimension reduction is to find a collection of matrices $\{\mathbf{V}^{(\ell)} \in \mathbb{R}^{P_\ell \times K_\ell}\}_{\ell=1}^L$ of rank $K_\ell \leq P_\ell$,

referred to as the mode- ℓ projection matrices, together with a center $\mathcal{C} \in \mathbb{R}^{P_1 \times \dots \times P_L}$ and core tensors $\{\mathcal{U}_n \in \mathbb{R}^{K_1 \times \dots \times K_L}\}_{n=1}^N$ such that the reconstructed tensors

$$\hat{\mathcal{X}}_n = \mathcal{C} + \mathcal{U}_n \times \{\mathbf{V}\}, \quad (2)$$

are a good approximation of the original tensors \mathcal{X}_n .

In Multilinear Principal Component Analysis the center equals the mean tensor $\mathcal{C} = \bar{\mathcal{X}} = \frac{1}{N} \sum_{n=1}^N \mathcal{X}_n$ whereas for fixed projection matrices $\mathbf{V}^{(\ell)}$ the core tensors are given by $\tilde{\mathcal{U}}_n = (\mathcal{X}_n - \bar{\mathcal{X}}) \times \{\mathbf{V}^T\} := \tilde{\mathcal{X}}_n \times \{\mathbf{V}^T\}$. The projection matrices are constrained to be orthogonal ($\mathbf{V}^{(\ell)T} \mathbf{V}^{(\ell)} = \mathbf{I}_{P_\ell}$) and are determined such that the resulting core tensors capture most of the variation observed in the original tensors, i.e. the total variation $\sum_{n=1}^N \|\tilde{\mathcal{U}}_n\|_F^2$ is maximized over all projection matrices $\mathbf{V}^{(\ell)}$. It can be shown that the solution also minimizes the sum of the squared reconstruction errors

$$\sum_{n=1}^N \left\| \mathcal{X}_n - \hat{\mathcal{X}}_n \right\|_F^2 = \sum_{n=1}^N \left\| \mathcal{X}_n - \mathcal{C} - \mathcal{U}_n \times \{\mathbf{V}\} \right\|_F^2. \quad (3)$$

The MPCA decomposition is illustrated in Figure 1. The projection matrices are common to all samples $\tilde{\mathcal{X}}_n$ while each of them reduces the dimension of one mode of the $\tilde{\mathcal{X}}_n$.

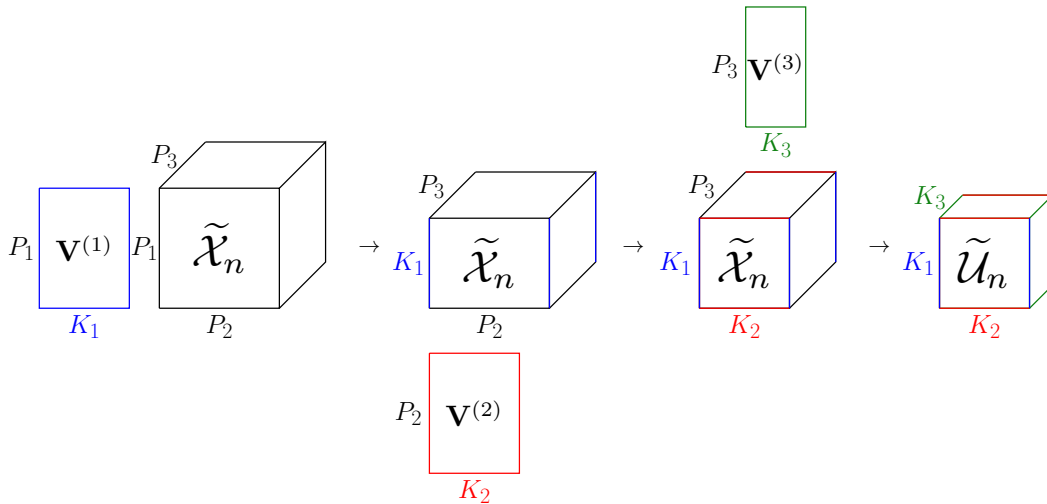


Figure 1: Illustration of the MPCA decomposition of a mean-centered tensor $\tilde{\mathcal{X}}_n$.

2.3 Robust MPCA

In this section we propose a new method for robust MPCA which can deal with casewise and cellwise outliers, as well as missing entries in the data. For each given \mathcal{X}_n , the tensor $\mathcal{M}_n = [m_{n,p_1 \dots p_L}]$ has value $m_{n,p_1 \dots p_L} = 1$ if $x_{n,p_1 \dots p_L}$ is observed, and 0 otherwise. The scalar $m_n = \sum_{p_1 \dots p_L} m_{n,p_1 \dots p_L}$ denotes the number of observed cells in \mathcal{X}_n and $m = \sum_{n=1}^N m_n$ the total number of observed cells in the set $\{\mathcal{X}_n\}$.

The proposed method ROMPCA estimates projection matrices $\mathbf{V}^{(\ell)} = [v_{p_\ell k_\ell}^{(\ell)}]$, core tensors $\mathcal{U}_n = [u_{n, k_1 \dots k_L}]$ and a robust center $\mathcal{C} = [c_{p_1 \dots p_L}]$ by minimizing

$$\mathcal{L}(\{\mathcal{X}_n\}, \{\mathbf{V}^{(\ell)}\}, \{\mathcal{U}_n\}, \mathcal{C}) := \frac{\hat{\sigma}_2^2}{m} \sum_{n=1}^N m_n \rho_2 \left(\frac{1}{\hat{\sigma}_2} \sqrt{\frac{1}{m_n} \sum_{p_1 \dots p_L}^{P_1 \dots P_L} m_{n, p_1 \dots p_L} \hat{\sigma}_{1, p_1 \dots p_L}^2 \rho_1 \left(\frac{r_{n, p_1 \dots p_L}}{\hat{\sigma}_{1, p_1 \dots p_L}} \right)} \right), \quad (4)$$

where the cellwise residuals are given by

$$r_{n, p_1 \dots p_L} := \left(x_{n, p_1 \dots p_L} - c_{p_1 \dots p_L} - \sum_{k_1 \dots k_L}^{K_1 \dots K_L} u_{n, k_1 \dots k_L} v_{p_1 k_1}^{(1)} \dots v_{p_L k_L}^{(L)} \right). \quad (5)$$

Each of the scales $\hat{\sigma}_{1, p_1 \dots p_L}$ standardizes the corresponding cellwise residuals $r_{n, p_1 \dots p_L}$ while the scale $\hat{\sigma}_2$ standardizes the casewise deviations

$$t_n := \sqrt{\frac{1}{m_n} \sum_{p_1 \dots p_L}^{P_1 \dots P_L} m_{n, p_1 \dots p_L} \hat{\sigma}_{1, p_1 \dots p_L}^2 \rho_1 \left(\frac{r_{n, p_1 \dots p_L}}{\hat{\sigma}_{1, p_1 \dots p_L}} \right)}. \quad (6)$$

If $\rho_1(z) = \rho_2(z) = z^2$ and there are no missing entries, the objective function (4) reduces to (3), the objective function minimized by MPCA. However, to handle both cellwise and casewise outliers simultaneously, we use bounded, even functions $\rho_1(z)$ and $\rho_2(z)$ in ROMPCA with $\rho_j(0) = 0$ and $\rho_j(z) > 0$ and nondecreasing for $z > 0$ ($j = 1, 2$). Specifically, ρ_1 is designed to mitigate cellwise outliers. The presence of cellwise outliers in the n th tensor would result in large absolute residuals $r_{n, p_1 \dots p_L}$, but their impact is tempered due to the boundedness of ρ_1 . Similarly, ρ_2 addresses casewise outliers. A casewise outlier leads to a large deviation t_n whose effect is then reduced by ρ_2 . Note that the presence of ρ_1 in t_n reduces the influence of outlying cells in the n th tensor and avoids that a single cellwise outlier would always result in a large t_n .

More precisely, in this paper both ρ -functions in (4) are chosen to be the hyperbolic tangent (*tanh*) (Hampel et al., 1981), defined by

$$\rho_{b,c}(z) = \begin{cases} z^2/2 & \text{if } 0 \leq |z| \leq b, \\ d - (q_1/q_2) \ln(\cosh(q_2(c - |z|))) & \text{if } b \leq |z| \leq c, \\ d & \text{if } c \leq |z|, \end{cases}$$

where $d = (b^2/2) + (q_1/q_2) \ln(\cosh(q_2(c - b)))$. Its derivative, denoted by $\psi_{b,c} = \rho'_{b,c}$, is

$$\psi_{b,c}(z) = \begin{cases} z & \text{if } 0 \leq |z| \leq b, \\ q_1 \tanh(q_2(c - |z|)) \operatorname{sign}(x) & \text{if } b \leq |z| \leq c, \\ 0 & \text{if } c \leq |z|. \end{cases}$$

The hyperbolic tangent ρ function and its derivative are shown in Figure 2 for the values $b = 1.5$, $c = 4$, $q_1 = 1.540793$ and $q_2 = 0.8622731$ advocated by Raymaekers and Rousseeuw (2021). Since $\psi_{1.5,4}(z) = 0$ for $|z| \geq 4$, large outlying cells and cases will be completely downweighted in the estimation procedure. See Section 2.4 for more details.

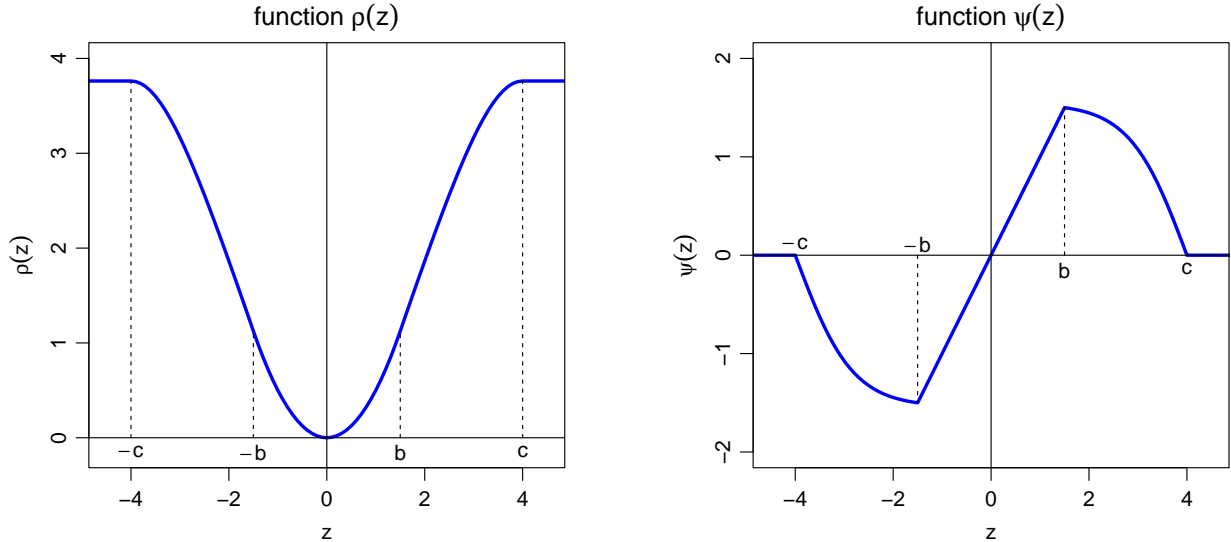


Figure 2: The function $\rho_{b,c}$ with $b = 1.5$ and $c = 4$ (left) and its derivative $\psi_{b,c}$ (right).

To correctly reduce the effect of both cellwise and casewise outliers, it is important that the scale estimates $\hat{\sigma}_{1,p_1\dots p_L}$ and $\hat{\sigma}_2$ in (4) are robust as well. Therefore, we will use M-scale estimators based on an initial fit as described in Section 2.5.

2.4 The ROMPCA Algorithm

To develop an algorithm to calculate the solution of (4), we first show that it is equivalent to a weighted least squares problem in the sense that they both yield the same first-order conditions. Since the loss function in (4) is continuously differentiable, we show in Section A of the Supplementary Material that its solution needs to satisfy the following first-order conditions

$$\sum_{n=1}^N \left\langle (\mathcal{X}_n - \mathcal{C} - \mathcal{U}_n \times \{\mathbf{V}\}) \odot \mathcal{W}_n, \mathcal{U}_n^{(-\ell)} \right\rangle_{\{L^*; L^*\}} = \mathbf{0}_{P_\ell \times K_\ell}, \quad \ell = 1, \dots, L \quad (7)$$

$$((\mathcal{X}_n - \mathcal{C} - \mathcal{U}_n \times \{\mathbf{V}\}) \odot \mathcal{W}_n) \times \{\mathbf{V}^T\} = \mathcal{O}_{K_1 \times \dots \times K_L}, \quad n = 1, \dots, N \quad (8)$$

$$\sum_{n=1}^N (\mathcal{X}_n - \mathcal{C} - \mathcal{U}_n \times \{\mathbf{V}\}) \odot \mathcal{W}_n = \mathcal{O}_{P_1 \times \dots \times P_L}, \quad (9)$$

where $L^* = \{1, \dots, \ell - 1, \ell + 1, \dots, L\}$. For each $n = 1 \dots N$, the weight tensor $\mathcal{W}_n = [w_{n,p_1 \dots p_L}]$ is defined as

$$\mathcal{W}_n = \mathcal{W}_n^{cell} \odot \mathcal{W}_n^{case} \odot \mathcal{M}_n, \quad (10)$$

where \mathcal{W}_n^{cell} and \mathcal{W}_n^{case} contain the cellwise and casewise weights, respectively. In particular, using the notation $\psi_i = \rho'_i$ for $i = 1, 2$, the tensor \mathcal{W}_n^{cell} has entries

$$w_{n,p_1 \dots p_L}^{cell} = \psi_1 \left(\frac{r_{n,p_1 \dots p_L}}{\hat{\sigma}_{1,p_1 \dots p_L}} \right) / \frac{r_{n,p_1 \dots p_L}}{\hat{\sigma}_{1,p_1 \dots p_L}}, \quad (11)$$

whereas \mathcal{W}_n^{case} is a tensor with the same value

$$w_n^{case} = \psi_2 \left(\frac{t_n}{\hat{\sigma}_2} \right) / \frac{t_n}{\hat{\sigma}_2}, \quad (12)$$

in each of its cells. We use the standard convention that the ratio $\psi(z)/z$ becomes 1 if $z = 0$ such that cells or cases with residual equal to 0 receive full weight 1. The conditions on the ρ functions guarantee that the weights $w_{n,p_1 \dots p_L} \geq 0$. We also assume that $\sum_{n=1}^N w_{n,p_1 \dots p_L}^q > 0$ for each entry, i.e. there is no entry whose value is contaminated or missing in all of the n samples. Note that for the hyperbolic tangent regular cells and cases (i.e. $\|z\| \leq b$) receive full weight 1 while strongly outlying cells and cases ($\|z\| \geq c$) receive weight 0.

For fixed weight tensors $\{\mathcal{W}_n\}$, equations (7)-(9) coincide with the first-order conditions of the weighted least squares problem

$$\sum_{n=1}^N \sum_{p_1 \dots p_L} w_{n,p_1 \dots p_L} \left(x_{n,p_1 \dots p_L} - c_{p_1 \dots p_L} - \sum_{k_1 \dots k_L}^{K_1 \dots K_L} u_{n,k_1 \dots k_L} v_{p_1 k_1}^{(1)} \cdots v_{p_L k_L}^{(L)} \right)^2, \quad (13)$$

as shown in Section A of the Supplementary Material. While there is no closed form solution of (13), the solution can be computed efficiently by alternating least squares (Gabriel, 1978). Since the weight tensors in (7)-(9) are not fixed but depend on the estimates, these equations can be solved by an Iteratively Reweighted Least Squares (IRLS) algorithm. The IRLS algorithm starts with an initial estimate $(\{\mathbf{V}_0^{(\ell)}\}, \{\mathcal{U}_{n,0}\}, \mathcal{C}_0)$ as explained in Section 2.5, and associated weight tensors $\{\mathcal{W}_{n,0}\}$ obtained from (10) by using the corresponding residuals (5) and (6) in the weights (11) and (12). Then, at each iteration step $q = 0, 1, 2, \dots$, updated estimates $\{\mathbf{V}_{q+1}^{(\ell)}\}, \{\mathcal{U}_{n,q+1}\}, \mathcal{C}_{q+1}$ and corresponding weight tensors $\{\mathcal{W}_{n,q+1}\}$ are obtained from the current estimates $\{\mathbf{V}_q^{(\ell)}\}, \{\mathcal{U}_{n,q}\}, \mathcal{C}_q$, and $\{\mathcal{W}_{n,q}\}$ by the following procedure, which is derived in Section B of the Supplementary Material.

- (a) First, (13) is minimized with respect to $\mathbf{V}^{(\ell)}$ by solving (7) for $\ell = 1, \dots, L$ which yields the

updated estimates

$$\text{vec} \left(\mathbf{V}_{q+1}^{(\ell)} \right) = \left(\sum_{n=1}^N \left(\mathbf{U}_{n(\ell),q}^{(-\ell)} \otimes \mathbf{I}_{P_\ell} \right) \mathbf{W}_{n,q} \left(\mathbf{U}_{n(\ell),q}^{(-\ell)} \otimes \mathbf{I}_{P_\ell} \right)^T \right)^\dagger \left(\sum_{n=1}^N \left(\mathbf{U}_{n(\ell),q}^{(-\ell)} \otimes \mathbf{I}_{P_\ell} \right) \mathbf{W}_{n,q} \text{vec} \left(\mathbf{X}_{n(\ell)} - \mathbf{C}_{(\ell),q} \right) \right), \quad (14)$$

where \dagger denotes the Moore-Penrose generalized inverse, $\mathbf{U}_{n(\ell),q}^{(-\ell)}$ is the mode- ℓ unfolding of $\mathcal{U}_{n,q}^{(-\ell)}$ and $\mathbf{C}_{(\ell),q}$ is the mode- ℓ unfolding of \mathcal{C}_q . The weight matrix $\mathbf{W}_{n,q}$ is defined such that every element of its diagonal is composed of the vectorization of $\mathcal{W}_{n,q}$. The matrix $\widetilde{\mathbf{W}}_{n,q}$ used below is similarly built from $\widetilde{\mathcal{W}}_{n,q} = \mathcal{W}_{n,q}^{\text{cell}} \odot \mathcal{M}_n$.

- (b) Using the updated estimates $\mathbf{V}_{q+1}^{(\ell)}$, (13) is then minimized with respect to \mathcal{U}_n by solving (8) for $n = 1, \dots, N$ which yields the updated estimates

$$\text{vec} (\mathcal{U}_{n,q+1}) = \left(\left(\bigotimes_{\ell=1}^L \mathbf{V}_{q+1}^{(\ell)T} \right) \widetilde{\mathbf{W}}_{n,q} \left(\bigotimes_{\ell=1}^L \mathbf{V}_{q+1}^{(\ell)} \right) \right)^\dagger \left(\left(\bigotimes_{\ell=1}^L \mathbf{V}_{q+1}^{(\ell)T} \right) \widetilde{\mathbf{W}}_{n,q} \text{vec} (\mathcal{X}_n - \mathcal{C}_q) \right). \quad (15)$$

- (c) Using the updated estimates $\mathbf{V}_{q+1}^{(\ell)}$ and $\mathcal{U}_{n,q+1}$, the center \mathcal{C} is then updated by solving (9) which yields

$$\mathcal{C}_{q+1} = \left(\sum_{n=1}^N (\mathcal{X}_n - \mathcal{U}_{n,q+1} \times \{\mathbf{V}_{q+1}\}) \odot \mathcal{W}_{n,q} \right) \odot \mathcal{H}_q, \quad (16)$$

where $\mathcal{H}_q = \left[1 / \sum_{n=1}^N w_{n,p_1 \dots p_L}^q \right] \in \mathbb{R}^{P_1 \times \dots \times P_L}$ with $w_{n,p_1 \dots p_L}^q$ the weights in $\mathcal{W}_{n,q}$.

- (d) Finally, the updated estimates $\{\mathbf{V}_{q+1}^{(\ell)}\}$, $\{\mathcal{U}_{n,q+1}\}$, and \mathcal{C}_{q+1} are used to update the residuals in (5) and (6), the corresponding weights (11) and (12) and weight tensor $\{\mathcal{W}_{n,q+1}\}$ in (10).

The algorithm iterates these steps until

$$\frac{\mathcal{L} \left(\{\mathcal{X}_n\}, \{\mathbf{V}_{q+1}^{(\ell)}\}, \{\mathcal{U}_{n,q+1}\}, \mathcal{C}_{q+1} \right) - \mathcal{L} \left(\{\mathcal{X}_n\}, \{\mathbf{V}_q^{(\ell)}\}, \{\mathcal{U}_{n,q}\}, \mathcal{C}_q \right)}{\mathcal{L} \left(\{\mathcal{X}_n\}, \{\mathbf{V}_q^{(\ell)}\}, \{\mathcal{U}_{n,q}\}, \mathcal{C}_q \right)} \leq 10^{-5}.$$

The following proposition implies that the IRLS algorithm to compute the ROMPCA estimates converges.

Proposition 1 *Each iteration step of the algorithm decreases the objective function (4), that is, $\mathcal{L} \left(\{\mathcal{X}_n\}, \{\mathbf{V}_{q+1}^{(\ell)}\}, \{\mathcal{U}_{n,q+1}\}, \mathcal{C}_{q+1} \right) \leq \mathcal{L} \left(\{\mathcal{X}_n\}, \{\mathbf{V}_q^{(\ell)}\}, \{\mathcal{U}_{n,q}\}, \mathcal{C}_q \right)$.*

The proof is given in Section C of the Supplementary Material, and uses the fact that for $z \geq 0$ the functions $z \rightarrow \rho_1(\sqrt{z})$ and $z \rightarrow \rho_2(\sqrt{z})$ are differentiable and concave. Since the objective function is decreasing and it has a lower bound of zero, the algorithm must converge.

2.5 Initialization

The use of the hyperbolic tangent as ρ -function makes the minimization of (4) a nonconvex optimization problem, which may have local minima. Therefore, the IRLS algorithm explained in the previous section may converge to a local minimum instead of the global minimum. To avoid that the algorithm converges to an undesirable non-robust local minimum, it is important that the initialization of the algorithm is chosen appropriately.

To obtain an initial fit for our IRLS algorithm, we construct two initialization candidates as follows. First we vectorize each tensor \mathcal{X}_n and stack the vectors rowwise into a matrix $\mathbf{X} = [\text{vec}(\mathcal{X}_1) \cdots \text{vec}(\mathcal{X}_N)]^T$. We apply the Detecting Deviating Cells (DDC) algorithm (Rousseeuw and Van den Bossche, 2018) to \mathbf{X} . DDC flags cellwise outliers (represented by an index set I_c) and provides imputed values for them. It also yields an index set I_r of potential casewise outliers. Note that these index sets are computed from the unfolded data and thus do not fully exploit the multiway structure of the data. Hence, they serve well for the construction of candidates to initialize the IRLS algorithm, but detection of cellwise and casewise outliers in the tensors will be based on the final ROMPCA solution (see Section 4 for details). We then select the $H = \lceil 0.75N \rceil$ tensors not in I_r with the fewest flagged cells in I_c and replace their outlying cells by the DDC imputed values. (If I_r contains more than 25% of the samples, then we select all the remaining tensors.) Standard MPCA is applied to these H imputed tensors $\{\mathcal{X}_h^{\text{DDC}}\}$, yielding initial estimates of $\{\mathbf{V}^{(\ell)}\}$ and \mathcal{C} . For all $n = 1, \dots, N$, initial cellwise weight tensors $\{\mathcal{W}_n^{\text{cell}}\}$ are obtained as well by setting the entries corresponding to elements of I_c equal to zero and all other entries equal to 1. Based on these initial estimates of $\{\mathbf{V}^{(\ell)}\}$, \mathcal{C} and $\{\mathcal{W}_n^{\text{cell}}\}$, initial estimates of $\{\mathcal{U}_n\}$ for all N tensors are then obtained from (15). This yields the estimates of the first initialization candidate.

To enhance robustness against cellwise outliers, a second initialization candidate is obtained by solving the objective function (4) with $\rho_1(x) = |x|$ and $\rho_2(x) = x^2$. To obtain this solution, the IRLS algorithm from Section 2.4 is applied, starting from the first initialization candidate explained above.

For both initialization candidates, the cellwise residuals are calculated using (5). Each of the corresponding cellwise scales $\hat{\sigma}_{1,p_1 \dots p_L}$ is then estimated by calculating a scale M-estimate of these cellwise residuals. A scale M-estimator of a univariate sample (z_1, \dots, z_n) is the solution $\hat{\sigma}$ of the equation

$$\frac{1}{n} \sum_{i=1}^n \rho \left(\frac{z_i}{a\sigma} \right) = \delta, \quad (17)$$

for a given δ . In this paper, the ρ -function in (17) is the hyperbolic tangent as before. The constant $\delta = 1.88$ for maximal robustness and $a = 0.3431$ for consistency at the standard Gaussian distribution. Based on the standardized cellwise residuals, the casewise deviations are then calculated using (6), and their M-scale $\hat{\sigma}_2$. The initial estimate $\left(\{\mathbf{V}_0^{(\ell)}\}, \{\mathcal{U}_{n,0}\}, \mathcal{C}_0 \right)$ to start the IRLS

algorithm of Section 2.4 is then the initialization candidate that yields the smallest scale estimate $\hat{\sigma}_2$.

2.6 Re-estimating the Center

Let $\{\mathbf{V}^{(\ell)}\}$, $\{\mathcal{U}_n\}$ and \mathcal{C} denote the estimates obtained by the IRLS algorithm of Section 2.4, yielding the fitted tensors $\hat{\mathcal{X}}_n = \mathcal{C} + \mathcal{U}_n \times \{\mathbf{V}\}$. For any $\mathcal{U}_0 \in \mathbb{R}^{K_1 \times \dots \times K_L}$, they can equivalently be computed as $\hat{\mathcal{X}}_n = \mathcal{C}^* + \mathcal{U}_n^* \times \{\mathbf{V}\}$, where $\mathcal{C}^* = \mathcal{C} + \mathcal{U}_0 \times \{\mathbf{V}\}$ and $\mathcal{U}_n^* = \mathcal{U}_n - \mathcal{U}_0$. This is known as the transitional ambiguity with respect to the center \mathcal{C} . If the primary focus of the analysis is on the fits $\hat{\mathcal{X}}_n$ or the core tensors $\{\mathcal{U}_n\}$, then this is not a concern. However, it does mean that the estimate \mathcal{C} does not necessarily represent the robust center of the tensors $\{\mathcal{X}_n\}$.

To obtain a meaningful estimate of the center, and thus facilitate interpretation, we can adjust the center \mathcal{C} based on the weighted average of the original tensors. In particular, we apply the transformation above for $\mathcal{U}_0 = (\bar{\mathcal{X}}^{\mathcal{W}} - \mathcal{C}) \times \{\mathbf{V}^T\}$ with

$$\bar{\mathcal{X}}^{\mathcal{W}} = \left(\sum_{n=1}^N \mathcal{X}_n \odot \mathcal{W}_n \right) \odot \mathcal{H},$$

where \mathcal{W}_n represents the final weight tensor (10) corresponding to the estimates $\{\mathbf{V}^{(\ell)}\}$, $\{\mathcal{U}_n\}$, and \mathcal{C} , and $\mathcal{H} = [1 / \sum_{n=1}^N w_{n,p_1 \dots p_L}]$. This yields the new center

$$\mathcal{C}^* = \mathcal{C} + (\bar{\mathcal{X}}^{\mathcal{W}} - \mathcal{C}) \times \{\mathbf{V}^T\} \times \{\mathbf{V}\},$$

and the core tensors are modified accordingly, i.e.

$$\mathcal{U}_n^* = \mathcal{U}_n - (\bar{\mathcal{X}}^{\mathcal{W}} - \mathcal{C}) \times \{\mathbf{V}^T\}.$$

The new estimates $\{\mathbf{V}^{(\ell)}\}$, $\{\mathcal{U}_n^*\}$ and \mathcal{C}^* are then reported as the final ROMPCA estimates.

2.7 Determining the Subspace Dimensions

Until now, the ranks K_ℓ , $\ell = 1, \dots, L$ of the projection matrices $\{\mathbf{V}^{(\ell)}\}$ were assumed fixed. However, in real applications, it is seldom the case that these ranks are known. For standard MPCA Lu et al. (2008) proposed the Q -based method to determine these ranks, which is a multilinear extension of the dimension selection strategy based on the cumulative percentage of total variation commonly used in PCA (Jolliffe, 2011). To determine the rank K_ℓ of $\mathbf{V}^{(\ell)}$, the Q -based method considers the ratio

$$Q^{(\ell)} = \frac{\sum_{p_\ell=1}^{K_\ell} \lambda_{p_\ell}^{(\ell)}}{\sum_{p_\ell=1}^{P_\ell} \lambda_{p_\ell}^{(\ell)}},$$

where $\lambda_{p_\ell}^{(\ell)}$ are the eigenvalues (in decreasing order) corresponding to the mode- ℓ unfolded scatter matrix $\mathbf{\Phi}^{(\ell)} = \sum_{n=1}^N (\mathbf{X}_{n^{(\ell)}} - \bar{\mathbf{X}}^{(\ell)}) (\mathbf{X}_{n^{(\ell)}} - \bar{\mathbf{X}}^{(\ell)})^T$. The $Q^{(\ell)}$ value thus measures the remaining portion of the mode- ℓ total scatter when removing the last $P_\ell - K_\ell$ components.

The rank for each mode may be chosen graphically by plotting the cumulative eigenvalues and determining the elbow point in this plot. Alternatively, it can be chosen as the smallest dimension K_ℓ for which $Q^{(\ell)}$ achieves a fixed threshold (e.g. 0.8), ensuring that the desired minimum explained variance is achieved. We cannot rely on the eigenvalues $\lambda_{p_\ell}^{(\ell)}$ of the unfolded scatter matrices estimates from $\{\mathcal{X}_n\}$ as they can be strongly affected by outliers and cannot deal with missing data. Therefore, we compute the eigenvalues from $\{\mathcal{X}_h^{\text{DPC}}\}$ defined in Section 2.5. Section D of the Supplementary Material illustrates the effectiveness of the proposed procedure on a simulated data set.

2.8 Imputed tensors

If a tensor \mathcal{X}_n has entries with cellwise weights strictly smaller than 1 and/or missing entries, we provide an imputed version $\mathcal{X}_n^{\text{imp}}$ of the tensor. Clearly, we do not want to modify entries of \mathcal{X}_n with weight $w_{n,p_1\dots p_L}^{\text{cell}} = 1$, hence $x_{n,p_1\dots p_L}^{\text{imp}} = x_{n,p_1\dots p_L}$ for these entries. The other entries of \mathcal{X}_n correspond to cellwise outliers or missing values and we use the ROMPCA solution to replace these entries by more regular values.

Equation (S.3) in the Supplementary Material can equivalently be written as

$$(\widetilde{\mathcal{W}}_n \odot (\mathcal{X}_n - \widehat{\mathcal{X}}_n)) \times \{\mathbf{V}^T\} = \mathcal{O}_{K_1 \times \dots \times K_L}.$$

Therefore, the imputed tensor is constructed as

$$\mathcal{X}_n^{\text{imp}} := \widehat{\mathcal{X}}_n + \widetilde{\mathcal{W}}_n \odot (\mathcal{X}_n - \widehat{\mathcal{X}}_n).$$

It then immediately follows from the previous equation that the multilinear projection of $\mathcal{X}_n^{\text{imp}}$ equals $\widehat{\mathcal{X}}_n$. Hence, \mathcal{X}_n and $\mathcal{X}_n^{\text{imp}}$ result in the same reconstructed tensor $\widehat{\mathcal{X}}_n$, but the imputed tensor has no missing or outlying entries and thus can be safely used in further analysis such as tensor regression or classification.

3 Simulation Study

In this section, we evaluate the empirical performance of ROMPCA in the presence of cellwise outliers and/or casewise outliers, both with and without missing values. The data generation process for the simulation study is inspired by Lu et al. (2008). Samples of 3-order tensors $\mathcal{X}_n \in \mathbb{R}^{P_1 \times P_2 \times P_3}$, $n = 1, \dots, N$, are generated according to the model $\mathcal{X}_n = \mathcal{U}_n \times_1 \mathbf{V}^{(1)} \times_2 \mathbf{V}^{(2)} \times_3 \mathbf{V}^{(3)} + \mathcal{E}_n$, where $\mathcal{U}_n \in \mathbb{R}^{K_1 \times K_2 \times K_3}$ are the core tensors, $\mathbf{V}^{(l)} \in \mathbb{R}^{P_l \times K_l}$, $l = 1, 2, 3$, are the mode- l projection matrices,

and $\mathcal{E}_n \in \mathbb{R}^{P_1 \times P_2 \times P_3}$ are noise tensors. The elements $u_{n,p_1 \dots p_L}$ of \mathcal{U}_n are drawn from the standard Gaussian distribution. These elements are then multiplied by $[(P_1, P_2, P_3)/(p_1 \cdot p_2 \cdot p_3)]^{0.9}$ to control the size of the eigenvalues. The columns of the matrices $\mathbf{V}^{(\ell)}$ are the eigenvectors corresponding to the K_ℓ largest eigenvalues of the $P_\ell \times P_\ell$ matrix $\Sigma^{(\ell)}$ with elements $\sigma_{i,j}^{(\ell)} = (-0.9)^{|i-j|}$. The entries of the noise tensor \mathcal{E}_n are sampled independently from a Gaussian distribution with zero mean and variance 0.1. We consider two settings: (i) $(P_1, P_2, P_3) = (30, 20, 5)$ and $(K_1, K_2, K_3) = (8, 6, 2)$, and (ii) $(P_1, P_2, P_3) = (15, 10, 5)$ and $(K_1, K_2, K_3) = (4, 3, 2)$. Because results for both scenarios are analogous, here we report only the results for setting (i) with higher dimensions. Section E of the Supplementary Material provides the results for setting (ii).

Three contamination scenarios are considered. In the cellwise outliers scenario, 20% of all $NP_1P_2P_3$ cells are randomly selected and each of these entries $x_{n,p_1 \dots p_L}$ is replaced by $\gamma_{cell}s_{p_1 \dots p_L}$, where $s_{p_1 \dots p_L}$ is the standard deviation of $\{x_{n,p_1 \dots p_L}\}_{n=1}^N$ and γ_{cell} ranges from 0 to 7. In the casewise outliers scenario, 20% of the N tensors are replaced by tensors generated from the model $\mathcal{X}_n^* = \mathcal{U}_n^* \times_1 \mathbf{V}^{*(1)} \times_2 \mathbf{V}^{*(2)} \times_3 \mathbf{V}^{*(3)} + \mathcal{E}_n$, where $\mathcal{U}_n^* \in \mathbb{R}^{(K_1+1) \times (K_2+1) \times (K_3+1)}$ is a tensor whose entries are 1 if all indices are odd and all other entries are set to zero. The columns of the matrices $\mathbf{V}^{(\ell)}$ for each mode are the first $K_\ell + 1$ odd-indexed eigenvectors of the matrix $\Sigma^{(\ell)}$ when ordered according to decreasing eigenvalues. This ensures that the resulting tensors have large variability along directions that differ from the bulk of the data. The resulting tensor \mathcal{X}_n^* is then multiplied by $\gamma_{case} = 3\gamma_{cell}$ where γ_{cell} ranges from 0 to 7 as before. In the combined scenario, the first 10% of tensors are replaced by casewise outliers as in the previous scenario. The remaining tensors are then contaminated by 10% of cellwise outliers as in the first scenario. Here, we set $\gamma_{case} = 6\gamma_{cell}$, where γ_{cell} again varies from 0 to 7. Note that the data are clean when $\gamma_{cell} = \gamma_{case} = 0$. When we consider settings with missing values, additionally, 10% of the entries are set completely at random to a missing value.

The performance is evaluated by the mean squared error (MSE) computed on the regular cells, given by

$$\text{MSE} = \sum_{n=1}^N \sum_{p_1 \dots p_L} \delta_{n,p_1 \dots p_L} (x_{n,p_1 \dots p_L} - \hat{x}_{n,p_1 \dots p_L})^2 / \sum_{n=1}^N \sum_{p_1 \dots p_L} \delta_{n,p_1 \dots p_L},$$

where $\delta_{n,p_1 \dots p_L}$ is 0 if \mathcal{X}_n is generated as a casewise outlier or if entry $x_{n,p_1 \dots p_L}$ is a generated cellwise outlier or missing entry, and $\delta_{n,p_1 \dots p_L}$ is 1 otherwise. We report for each scenario the median MSE over 50 samples of $N = 100$ observations for each of the methods as a function of the outlier size γ_{cell} .

First, we consider settings without missing values. ROMPCA is compared to standard MPCA and to two alternative methods that are related to the methods proposed by Inoue et al. (2009) that are designed to address either casewise or cellwise outliers, but not both at the same time. Both methods can be seen as special cases of ROMPCA. The first one, OnlyCase-MPCA, uses $\rho_1(z) = z^2$ and the second method, OnlyCell-MPCA, has $\rho_2(z) = z^2$. In our simulations it turned

out that they yielded more robust results than the original proposals of Inoue et al. (2009).

Figure 3 shows the median MSE of the four methods for all three contamination scenarios. Without contamination ($\gamma_{cell} = 0$ in the plots of Figure 3), standard MPCA slightly outperforms all other methods, as expected. From the left plot of Figure 3, it can be seen that MPCA and OnlyCase-MPCA are highly affected by the presence of cellwise contamination, while ROMPCA and OnlyCell-MPCA show a much more robust behavior. Cellwise outliers have a slight effect on these methods when they are close by, but this effect quickly disappears when the cellwise outliers are more distinct from the regular measurements.

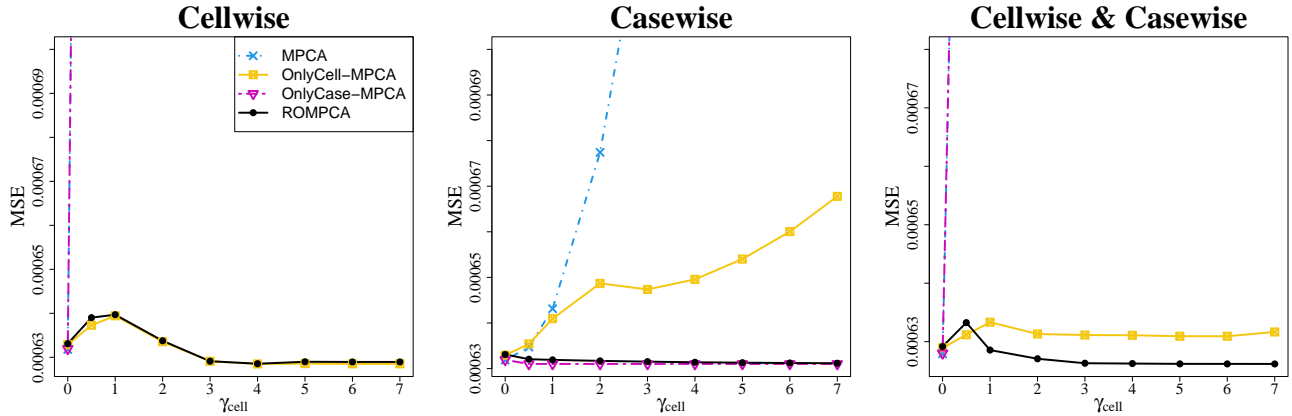


Figure 3: Median MSE attained by MPCA, OnlyCase-MPCA, OnlyCell-MPCA, and ROMPCA under cellwise contamination, casewise contamination or both in function of γ_{cell} for data without missing values.

The middle plot of Figure 3) shows that standard MPCA also cannot resist casewise outliers. OnlyCell-MPCA also struggles to resist the effect of this type of contamination for which it is not designed. In contrast, both ROMPCA and OnlyCase-MPCA are hardly affected by the presence of casewise contamination with OnlyCase-MPCA performing slightly better than ROMPCA in this case.

When both cellwise outliers and casewise outliers are present, ROMPCA generally outperforms all other methods as soon as the outliers are distinguishable from the regular data. As expected, the other methods do not perform well in this setting, either because they are not robust to cellwise outliers (OnlyCase-MPCA), casewise outliers (OnlyCell-MPCA), or both (MPCA).

Figure 4 shows the MSE results for the same contamination scenarios when also missing values are added. Standard MPCA is not included in this comparison as this method cannot cope with missing values. Comparing these results with Figure 3, it can be seen that the presence of missing values generally has little effect on the performance of the methods. Overall, ROMPCA shows the best behavior across all scenarios.

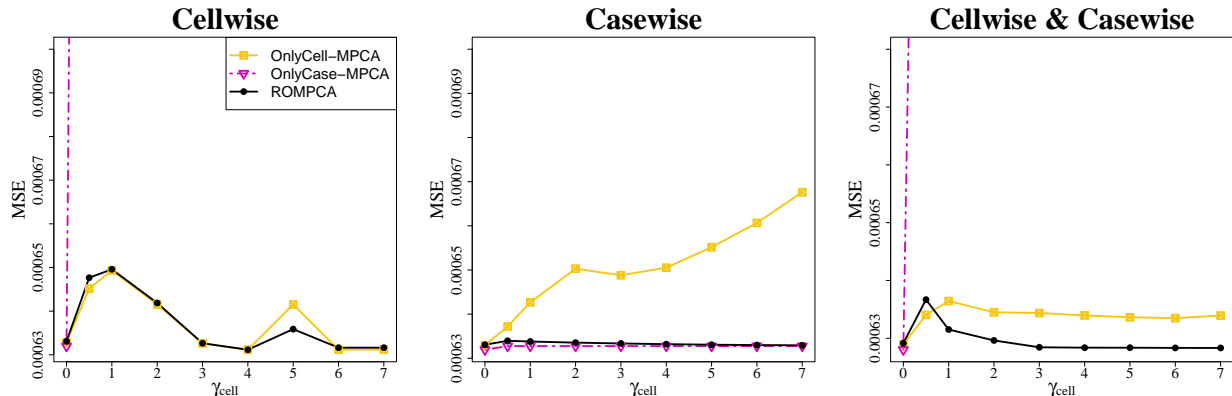


Figure 4: Median MSE attained by OnlyCase-MPCA, OnlyCell-MPCA, and ROMPCA under cellwise contamination, casewise contamination or both in function of γ_{cell} for data with 10% of missing values.

4 Outlier Detection

Based on the ROMPCA estimates we can construct numerical and graphical diagnostics to gain more insight into the outlying cells and anomalous cases in the data. First the scale estimates $\hat{\sigma}_{1,p_1\dots p_L}$ are recomputed as M-scales $\tilde{\sigma}_{p_1\dots p_L}$ of the ROMPCA cellwise residuals (5). This yields for each observation its final standardized residual tensor $\tilde{\mathcal{R}}_n = [\tilde{r}_{n,p_1\dots p_L}] = [r_{n,p_1\dots p_L}/\tilde{\sigma}_{p_1\dots p_L}]$.

The residual cellmap is a heatmap which visualizes the cellwise outlyingness of entries in the data (Rousseeuw and Van den Bossche, 2018; Hubert and Hirari, 2024). Standardized cellwise residuals whose absolute value is smaller than the threshold $c_{cell} = \sqrt{\chi_{1,0.998}^2} = 3.09$ are considered to be regular and are colored yellow. The other cells are flagged as cellwise outliers. To indicate their direction and degree of outlyingness, cells with positive standardized cellwise residual exceeding c_{cell} are colored from light orange to red, while cells with negative standardized cellwise residual below $-c_{cell}$ are colored from purple to dark blue. Cells whose value is missing are colored white.

We can display a residual cellmap of all individual data cells by vectorizing each observed tensor and stacking these vectors rowwise into a matrix (as in Section 2.5). As this may result in a very wide matrix (if $\prod_{\ell=1}^L P_\ell$ is large), it is possible to aggregate adjacent cells and display the average color. As an illustration, let us consider a data set with $N = 100$ simulated tensors according to the setting of Section 3 with $(P_1, P_2, P_3) = (15, 10, 5)$. We leave 10 out of the 100 tensors completely uncontaminated, change 10 tensors into casewise outliers and then contaminate the remaining cells with 10% of cellwise outliers and 1% of missing values. We use $\gamma_{cell} = 5$ and $\gamma_{case} = 6\gamma_{cell}$.

Figure 5 shows the residual cellmap for this data set, where each cell has the average color of two columns of the vectorized tensors. The 10 outlying cases are clearly visible by the horizontal lines with mostly outlying cells.

While this residual cellmap makes it possible to easily identify cases with many cellwise outliers,

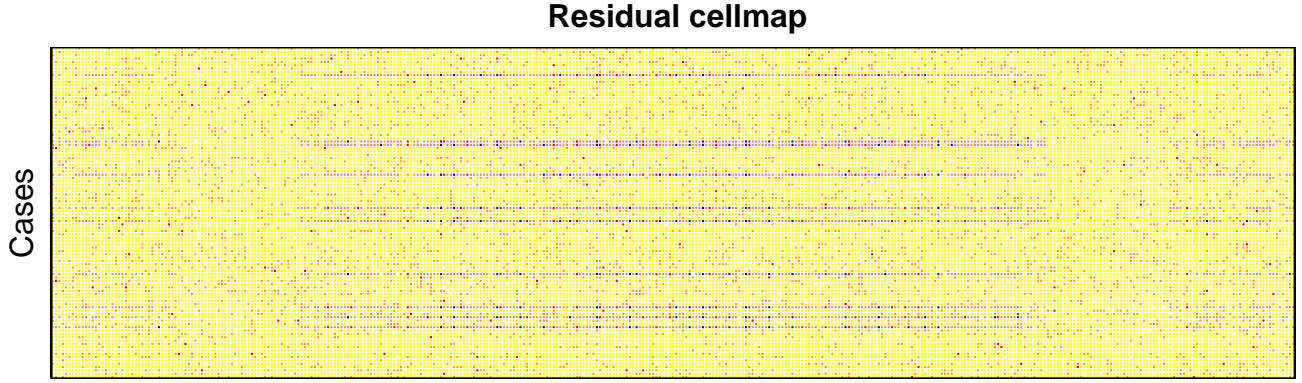


Figure 5: Residual cellmap of a simulated data set with aggregated columns.

the high dimensionality of this matrix and/or the merging of columns makes it difficult to identify the positions of cellwise outliers in the data tensors. A more detailed insight is provided by making residual cellmaps of slices of the standardized residual tensors. This is illustrated in Figure 6, which shows the residual cellmaps of slices from the 3th mode of the standardized residual tensors corresponding to four different observations. The first observation is an uncontaminated tensor, the second one has cellwise outliers, the third one additionally has missing values while the fourth tensor is a casewise outlier.

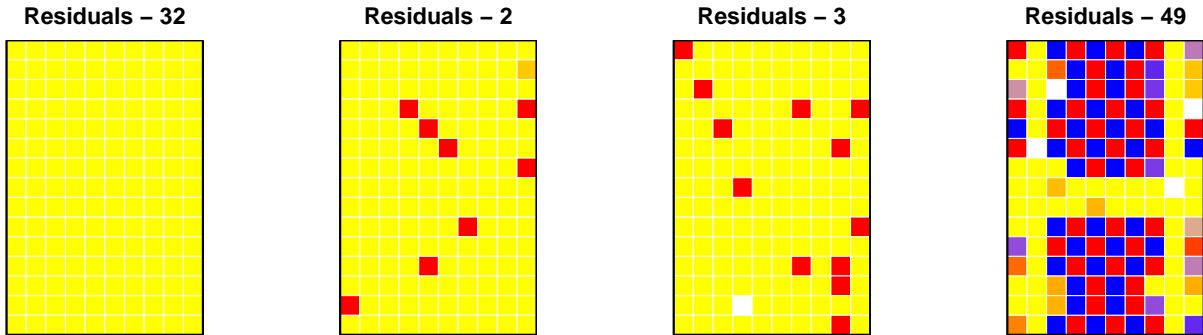


Figure 6: Residual cellmaps of slices from the 3th mode of four observations from the simulated data set.

To focus more on the casewise outlyingness of the observed tensors, a new residual plot is proposed based on the ROMPCA fit. It displays (on the log scale) the observations' residual distance, defined as $\|\tilde{\mathcal{R}}_n\|_F$, versus their index. The size of each point in this plot is proportional to the Percentage of Outlying Cells (POC) in the observation, which for each observation is defined as

$$\text{POC}_n = \frac{1}{\prod_{\ell} P_{\ell}} \sum_{p_1 \dots p_L}^{P_1 \dots P_L} I(|\tilde{r}_{n,p_1 \dots p_L}| > c_{\text{cell}}),$$

where I is the indicator function (Hubert and Hirari, 2024). Larger points thus correspond to

observations with many outlying cells. Finally, points are colored based on their casewise weight. To be consistent with the residual cellmap, the color is yellow when $w_n^{case} = 0$, red when $w_n^{case} = 1$, and orange for intermediate weights. The red horizontal dotted line is the cutoff c_{case} , i.e., the 0.99-quantile of the distribution of $\|\tilde{\mathcal{R}}_n\|_F$ for uncontaminated errors. In particular, a large set of tensors of the same size as $\tilde{\mathcal{R}}_n$ with standard normal entries is generated. The 0.99 quantile of their Frobenius norms is then calculated to obtain c_{case} . Cases with a residual distance smaller than c_{case} are considered to be regular observations. Figure 7 shows the residual distance plot for the simulated data set of Figure 5. We can clearly distinguish cases with contamination (above the cutoff line) from the regular cases. The difference between tensors with cellwise outliers on the one hand and casewise outliers on the other hand is also clearly seen from the color and size of the points.

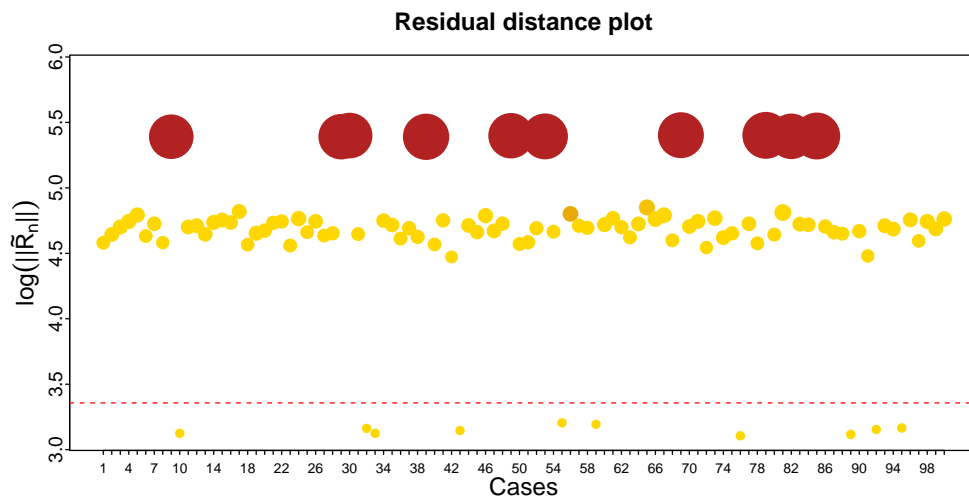


Figure 7: Plot of the ROMPCA residual distances for a simulated data set.

5 Real Data Examples

5.1 Dog Walker Data

The Dog Walker data (<https://www.wisdom.weizmann.ac.il/~vision/SpaceTimeActions.html>) consists of surveillance video data of a man walking his dog. The video was filmed using a static camera and consists of 54 colored frames. Each frame has (144×180) pixels and is stored using the RGB (Red, Green, Blue) color model. For the sake of computation time, every frame is down-sampled by image decimation such that it has (72×90) pixels. The upper row of Figure 8 shows four frames from the video.

This data set can be represented as a collection of 3-order tensors, where the first two modes

correspond to the pixel space, while the third mode corresponds to the color space. We approximate the data tensors according to the following decomposition

$$\hat{\mathcal{X}}_n = \mathcal{C} + \mathcal{U}_n \times_1 \mathbf{V}^v \times_2 \mathbf{V}^h \times_3 \mathbf{V}^{\text{col}}.$$

Here, \mathbf{V}^{col} denotes the projection matrix for the color space. \mathbf{V}^v and \mathbf{V}^h denote the projection matrices for the vertical axis and horizontal axis of the pixel space, respectively. The ranks are chosen equal to $(1, 1, 1)$ based on a plot of the cumulative eigenvalues as explained in Section 2.7. See Section F of the Supplementary Material for more details.

In Figure 8, the observed frames are compared to the fitted frames using ROMPCA. It can immediately be seen that the man walking the dog does not appear anymore on the fitted frames. In this setting, the man walking his dog is successfully identified as outlying as it is the only part that significantly changes in the successive frames.



Figure 8: Frames from the Dog Walker data (upper row) and reconstructed frames using ROMPCA (lower row).

Figure 9 shows the ROMPCA residual cellmap where each column in this map corresponds to 100 aggregated columns. We clearly see a diagonal pattern of cellwise outliers that corresponds to the man walking his dog who changes position in each of the frames.

For a more detailed view, we look at the residual cellmap of some slices. Figure 10 shows the residual cellmap for the blue color slice of four frames. In these residual cellmaps, we can clearly see that most of the cellwise outliers correspond to the man walking his dog. The first frames also show numerous deviating cells in the background. They mostly result from the wind moving the tree leaves.

Finally we take a closer look at the core tensors, that here, consist of scalars. They are displayed in Figure 11 and clearly show a non-constant pattern, mostly in the first half. Thus, the background

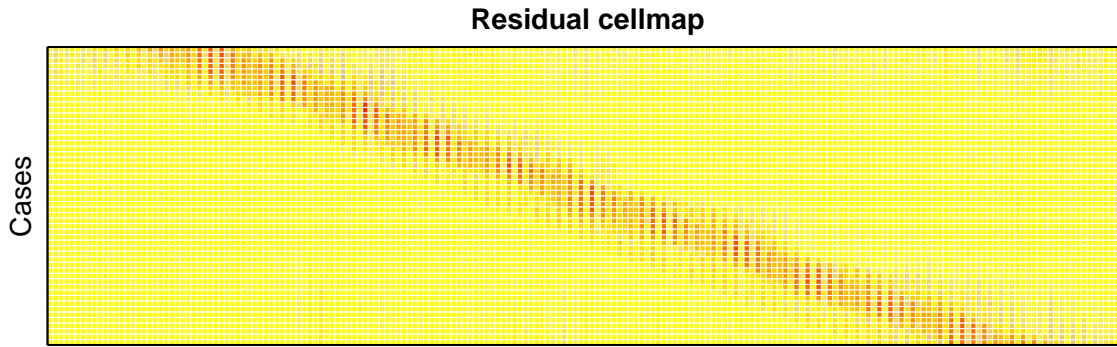


Figure 9: ROMPCA residual cellmap of the Dog Walker data set.

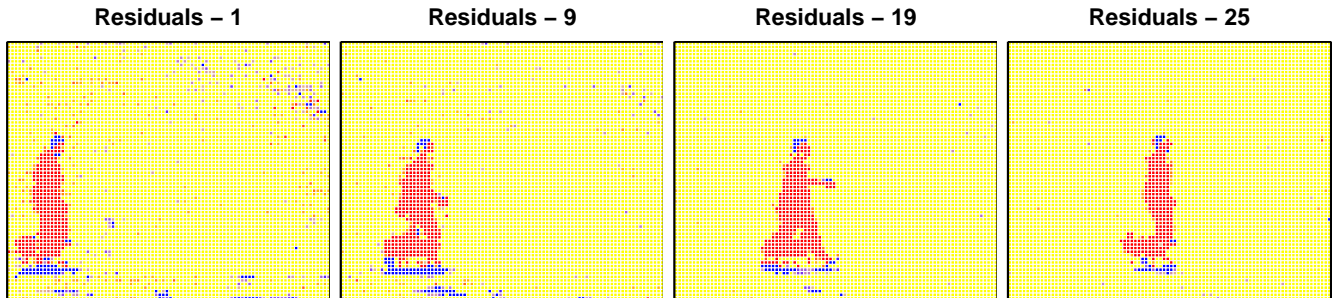


Figure 10: ROMPCA residual cellmaps of several slices (corresponding to the blue color) of the Dog Walker data.

is not constant, as one might initially suspect from watching the video. ROMPCA has detected that there is smooth change in the illumination.

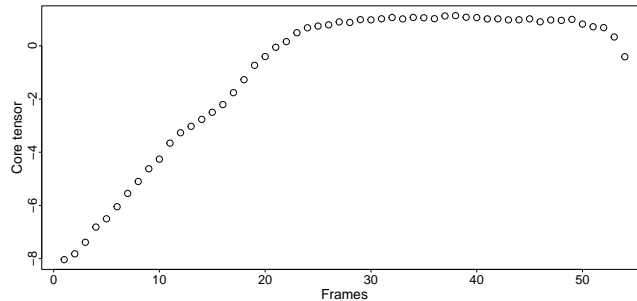


Figure 11: ROMPCA core tensors of the Dog Walker data.

Section F of the Supplementary Material contains more results for this example. There, we show that MPCA is not able to clearly distinguish the man from the background. Furthermore, we also show that DDC applied to the vectorized tensors does not capture the change in the illumination. A multilinear approach is thus better in modeling this variation.

5.2 Dorrit Data

As a second example, we consider the Dorrit data set (Baunsgaard, 1999). Data are laboratory-generated and consist of 27 different mixtures of fluorophores (hydroquinone, tryptophan, phenylalanine and dopa). For each mixture, the Excitation Emission Matrix (EEM) is measured with emission wavelengths from 250 nm to 482 nm at 2 nm intervals, and excitation wavelengths from 230 nm to 315 nm at 5 nm intervals. This yields a collection of 27 matrices of size 116×18 . Samples 2, 3, and 5 are known to be highly anomalous observations. They have very high concentrations for some fluorophores, resulting in large intensities and missing entries. Data are preprocessed to remove the Rayleigh and Raman scattering that affects all samples (see e.g. Engelen et al., 2007).

The plot of the cumulative eigenvalues (see Section G of the Supplementary Material) suggests to choose the ranks $(K_1, K_2) = (4, 4)$. This is in line with the ranks used by Goldfarb and Qin (2014) in their analysis.

Figure 12 shows the ROMPCA residual cellmap where cells in adjacent columns have been aggregated such that the first 8 columns in the residual map correspond to the emission wavelengths at an excitation wavelength of 230 nm, the next 8 columns correspond to an excitation wavelength of 235 nm, and so on. This results in 18 blocks, which are separated by thin green lines. We see that ROMPCA has identified cellwise outliers in many observations, but mostly in the cases 2, 3 and 5.

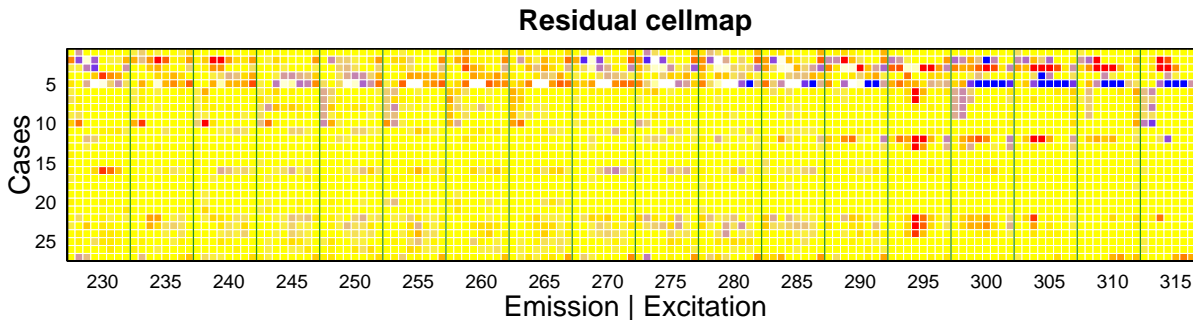


Figure 12: ROMPCA residual cellmap of the Dorrit data.

These three observations also most pronounced stand out in the residual distance plot in Figure 13. Five more mixtures are colored red and thus flagged as casewise outliers. They contain a substantial fraction of cells that are mildly outlying. Only 7 mixtures are found to be regular. The remaining mixtures exceed the cutoff as they contain cellwise outliers which enlarges their residual distance.

Following Goldfarb and Qin (2014) we next apply a PARAFAC decomposition to the ROMPCA fitted matrices $\hat{\mathcal{X}}_n$ that correspond to the $\tilde{N} = 19$ cases with a casewise weight of 1. We construct the 3-order tensor $\tilde{\mathcal{X}}$ where the first mode represents the observations, so $\tilde{\mathcal{X}}_{\tilde{n},:,;} = \hat{\mathcal{X}}_{\tilde{n}}$ for $\tilde{n} =$

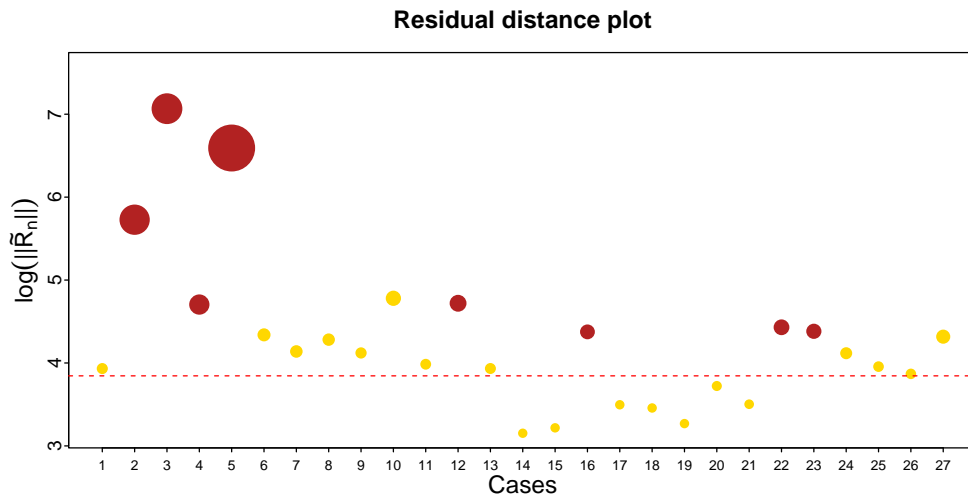


Figure 13: Plot of the ROMPCA residual distances of the Dorrit data.

$1, \dots, \tilde{N}$. The PARAFAC model decomposes this tensor into the sum of F rank-1 tensors:

$$\tilde{\mathcal{X}} \approx \sum_{j=1}^F \mathbf{a}_j \otimes \mathbf{b}_j \otimes \mathbf{c}_j$$

where \otimes denotes the outer product between vectors. Here we take $F = 4$ since it is known that the mixture is composed of four fluorophores. The emission \mathbf{b}_f and excitation profiles \mathbf{c}_f of pure samples were obtained earlier and serve as a reference (Baunsgaard, 1999). Figure 14 compares the estimated emission and excitation loadings (solid lines) with the benchmark loadings (dotted lines). It can be seen that all loading vectors are well aligned with the pure loadings. ROMPCA has thus been able to extract well the main structure from the data, and to provide an outlier-free reconstructed EEM data set to which PARAFAC could be applied.

In contrast, Figure 15 shows the estimated emission and excitation loadings (solid lines) obtained from the PARAFAC decomposition of the standard MPCA fitted tensors. They are clearly highly distorted by the outlying measurements.

6 Conclusion

We proposed a novel robust MPCA method for tensor data, the first to simultaneously handle casewise and cellwise outliers, along with missing values. Its objective function combines two robust loss functions to reduce the effect of cellwise and casewise outliers, respectively.

The ROMPCA fit can be computed via an iteratively reweighted least squares algorithm which uses alternating weighted least squares as its building block. The algorithm yields cellwise and casewise weights, which, together with the standardized cellwise residuals, can be used to construct graphical outlier detection tools. We developed residual cellmaps and a residual distance

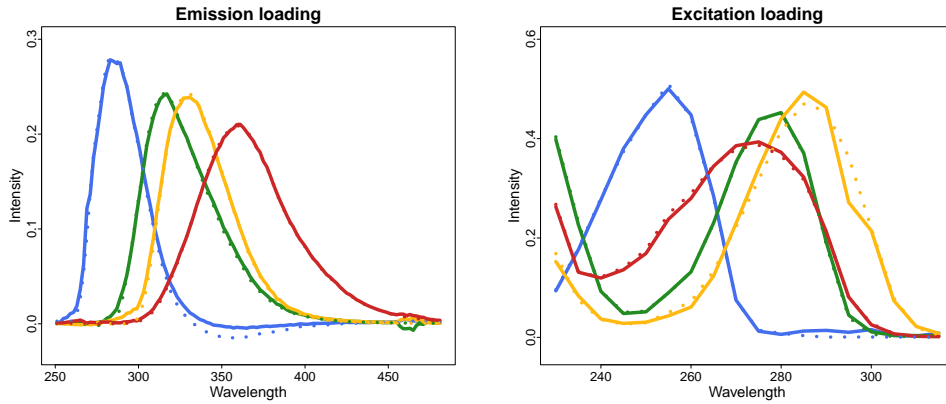


Figure 14: Emission (left) and excitation (right) loadings for the Dorrit dataset. The solid lines represent the estimated loadings based on ROMPCA, while the dotted lines indicate the pure loadings.

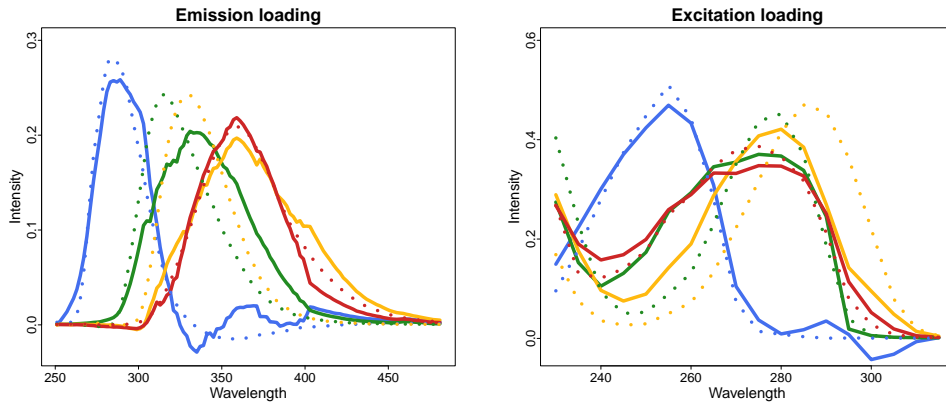


Figure 15: Emission (left) and excitation (right) loadings for the Dorrit dataset. The solid lines represent the estimated loadings based on MPCA, while the dotted lines indicate the pure loadings.

plot to visualize both types of outliers. The good performance of ROMPCA is demonstrated via simulations and applications to real datasets.

Another advantage of ROMPCA is that it also returns imputed tensors in which the missing and outlying entries have been replaced by imputed values. If the original tensors are replaced by these imputed tensors in further analysis such as tensor regression or classification, then standard methods, which cannot handle missing data and are not robust, can be applied directly.

References

Alqallaf, F., S. Van Aelst, V. J. Yohai, and R. H. Zamar (2009). Propagation of outliers in multivariate data. *The Annals of Statistics*, 311–331.

- Baunsgaard, D. (1999). *Factors affecting 3-way modelling (PARAFAC) of fluorescence landscapes*. Ph. D. thesis, Royal Veterinary and Agricultural University, Department of Dairy and Food technology, Frederiksberg, Denmark.
- Carroll, J. D. and J.-J. Chang (1970). Analysis of individual differences in multidimensional scaling via an n-way generalization of “Eckart-Young” decomposition. *Psychometrika* 35(3), 283–319.
- Centofanti, F., M. Hubert, and P. J. Rousseeuw (2024). Robust principal components by casewise and cellwise weighting. *arXiv preprint arXiv:2408.13596*.
- Croux, C. and A. Ruiz-Gazen (2005). High breakdown estimators for principal components: the projection-pursuit approach revisited. *Journal of Multivariate Analysis* 95, 206–226.
- De La Torre, F. and M. J. Black (2003). A framework for robust subspace learning. *International Journal of Computer Vision* 54, 117–142.
- De Lathauwer, L., B. De Moor, and J. Vandewalle (2000). A multilinear singular value decomposition. *SIAM journal on Matrix Analysis and Applications* 21(4), 1253–1278.
- Engelen, S., S. Frosch Møller, and M. Hubert (2007). Automatically identifying scatter in fluorescence data using robust techniques. *Chemometrics and Intelligent Laboratory Systems* 86, 35–51.
- Engelen, S. and M. Hubert (2011). Detecting outlying samples in a parallel factor analysis model. *Analytica Chimica Acta* 705(1-2), 155–165.
- Gabriel, K. R. (1978). Least squares approximation of matrices by additive and multiplicative models. *Journal of the Royal Statistical Society Series B* 40(2), 186–196.
- Goldfarb, D. and Z. Qin (2014). Robust low-rank tensor recovery: Models and algorithms. *SIAM Journal on Matrix Analysis and Applications* 35(1), 225–253.
- Hampel, F. R., P. J. Rousseeuw, and E. Ronchetti (1981). The change-of-variance curve and optimal redescending M-estimators. *Journal of the American Statistical Association* 76(375), 643–648.
- Han, J. and B. Bhanu (2005). Individual recognition using gait energy image. *IEEE Transactions on Pattern Analysis and Machine Intelligence* 28(2), 316–322.
- Harshman, R. A. (1970). Foundations of the PARAFAC procedure: Models and conditions for an “explanatory” multi-modal factor analysis. *UCLA working papers in phonetics* 16(1), 84.

- Hubert, M. and M. Hirari (2024). MacroPARAFAC for handling rowwise and cellwise outliers in incomplete multiway data. *Chemometrics and Intelligent Laboratory Systems* 251, 105170.
- Hubert, M., P. J. Rousseeuw, and W. Van den Bossche (2019). MacroPCA: An all-in-one PCA method allowing for missing values as well as cellwise and rowwise outliers. *Technometrics* 61, 459–473.
- Hubert, M., P. J. Rousseeuw, and K. Vanden Branden (2005). ROBPCA: a new approach to robust principal component analysis. *Technometrics* 47, 64–79.
- Hubert, M., J. Van Kerckhoven, and T. Verdonck (2012). Robust PARAFAC for incomplete data. *Journal of Chemometrics* 26, 290–298.
- Inoue, K., K. Hara, and K. Urahama (2009). Robust multilinear principal component analysis. In *2009 IEEE 12th International Conference on Computer Vision*, pp. 591–597.
- Jolliffe, I. (2011). *Principal Component Analysis*. Springer.
- Kolda, T. G. (2006). Multilinear operators for higher-order decompositions. Technical Report SAND2006-2081, Sandia National Laboratories.
- Kroonenberg, P. M. (2008). *Applied multiway data analysis*. Wiley Series in Probability and Statistics. Hoboken, NJ: Wiley-Interscience.
- Liu, Y., F. Shang, W. Fan, J. Cheng, and H. Cheng (2015). Generalized higher order orthogonal iteration for tensor learning and decomposition. *IEEE transactions on neural networks and learning systems* 27(12), 2551–2563.
- Locantore, N., J. Marron, D. Simpson, N. Tripoli, J. Zhang, K. Cohen, G. Boente, R. Fraiman, B. Brumback, C. Croux, et al. (1999). Robust principal component analysis for functional data. *Test* 8, 1–73.
- Lu, H., K. N. Plataniotis, and A. N. Venetsanopoulos (2008). MPCA: Multilinear principal component analysis of tensor objects. *IEEE Transactions on Neural Networks* 19(1), 18–39.
- Maronna, R. A. and V. J. Yohai (2008). Robust low-rank approximation of data matrices with elementwise contamination. *Technometrics* 50(3), 295–304.
- Raymaekers, J. and P. J. Rousseeuw (2021). Fast robust correlation for high-dimensional data. *Technometrics* 63(2), 184–198.
- Rousseeuw, P. J. and W. Van den Bossche (2018). Detecting deviating data cells. *Technometrics* 60, 135–145.

- Sarkar, S., P. J. Phillips, Z. Liu, I. R. Vega, P. Grother, and K. W. Bowyer (2005). The humanid gait challenge problem: Data sets, performance, and analysis. *IEEE Transactions on Pattern Analysis and Machine Intelligence* 27(2), 162–177.
- Serneels, S. and T. Verdonck (2008). Principal component analysis for data containing outliers and missing elements. *Computational Statistics & Data Analysis* 52(3), 1712–1727.
- Shi, Q., Y.-M. Cheung, Q. Zhao, and H. Lu (2018). Feature extraction for incomplete data via low-rank tensor decomposition with feature regularization. *IEEE Transactions on Neural Networks and Learning Systems* 30(6), 1803–1817.
- Smilde, A., R. Bro, and P. Geladi (2004). *Multi-way Analysis with Applications in the Chemical Sciences*. England: Wiley.
- Todorov, V., V. Simonacci, M. Gallo, and N. Trendafilov (2023). A novel estimation procedure for robust CANDECOMP/PARAFAC model fitting. *Econometrics and Statistics*.
- Tucker, L. R. (1966). Some mathematical notes on three-mode factor analysis. *Psychometrika* 31(3), 279–311.
- Vasilescu, M. A. O. and D. Terzopoulos (2007). Multilinear projection for appearance-based recognition in the tensor framework. In *2007 IEEE 11th International Conference on Computer Vision*, pp. 1–8.
- Ye, J., R. Janardan, and Q. Li (2004). GPCA: An efficient dimension reduction scheme for image compression and retrieval. In *Proceedings of the tenth ACM SIGKDD international conference on Knowledge discovery and data mining*, pp. 354–363.
- Zhao, Q., L. Zhang, and A. Cichocki (2015). Bayesian CP factorization of incomplete tensors with automatic rank determination. *IEEE Transactions on Pattern Analysis and Machine Intelligence* 37(9), 1751–1763.

Supplementary Materials to:
Robust Multilinear Principal Component Analysis

Mehdi Hirari, Fabio Centofanti, Mia Hubert, Stefan Van Aelst

A First-Order Conditions

In the following, the derivation of the first-order necessary conditions (7)-(9) is presented. The objective function is given by

$$\mathcal{L}(\{\mathcal{X}_n\}, \{\mathbf{V}^{(\ell)}\}, \{\mathcal{U}_n\}, \mathcal{C}) = \frac{\hat{\sigma}_2^2}{m} \sum_{n=1}^N m_n \rho_2 \left(\frac{1}{\hat{\sigma}_2} \sqrt{\frac{1}{m_n} \sum_{p_1 \dots p_L}^{P_1 \dots P_L} m_{n,p_1 \dots p_L} \hat{\sigma}_{1,p_1 \dots p_L}^2 \rho_1 \left(\frac{r_{n,p_1 \dots p_L}}{\hat{\sigma}_{1,p_1 \dots p_L}} \right)} \right),$$

The derivative of \mathcal{L} with respect to $v_{p_\ell k_\ell}^{(\ell)}$ is

$$\begin{aligned} \frac{\partial \mathcal{L}}{\partial v_{p_\ell k_\ell}^{(\ell)}} &= \frac{\hat{\sigma}_2^2}{m} \sum_{n=1}^N m_n \rho_2' \left(t_n / \hat{\sigma}_2 \right) \frac{1}{\hat{\sigma}_2} \frac{\partial}{\partial v_{p_\ell k_\ell}^{(\ell)}} \sqrt{\frac{1}{m_n} \sum_{p_1 \dots p_L}^{P_1 \dots P_L} m_{n,p_1 \dots p_L} \hat{\sigma}_{1,p_1 \dots p_L}^2 \rho_1 \left(\frac{r_{n,p_1 \dots p_L}}{\hat{\sigma}_{1,p_1 \dots p_L}} \right)} \\ &= \frac{1}{2m} \sum_{n=1}^N \frac{\psi_2(t_n / \hat{\sigma}_2)}{t_n / \hat{\sigma}_2} \frac{\partial}{\partial v_{p_\ell k_\ell}^{(\ell)}} \left(\sum_{p_1 \dots p_L}^{P_1 \dots P_L} m_{n,p_1 \dots p_L} \hat{\sigma}_{1,p_1 \dots p_L}^2 \rho_1 \left(\frac{r_{n,p_1 \dots p_L}}{\hat{\sigma}_{1,p_1 \dots p_L}} \right) \right) \\ &= \frac{1}{2m} \sum_{n=1}^N w_n^{case} \sum_{p_\ell, \ell \in L^*} \hat{\sigma}_{1,p_1 \dots p_L}^2 \psi_1(r_{n,p_1 \dots p_L} / \hat{\sigma}_{1,p_1 \dots p_L}) \frac{m_{n,p_1 \dots p_L}}{\hat{\sigma}_{1,p_1 \dots p_L}} \frac{\partial r_{n,p_1 \dots p_L}}{\partial v_{p_\ell k_\ell}^{(\ell)}} \\ &= -\frac{1}{2m} \sum_{n=1}^N \sum_{p_\ell, \ell \in L^*} \left[w_n^{case} w_{n,p_1 \dots p_L}^{cell} m_{n,p_1 \dots p_L} r_{n,p_1 \dots p_L} \right. \\ &\quad \left. \sum_{k_\ell, \ell \in L^*} \left(u_{n,k_1 \dots k_L} v_{p_1 k_1}^{(1)} \dots v_{p_{\ell-1} k_{\ell-1}}^{(\ell-1)} v_{p_{\ell+1} k_{\ell+1}}^{(\ell+1)} \dots v_{p_L k_L}^{(L)} \right) \right], \end{aligned}$$

where $L^* = \{1, \dots, \ell - 1, \ell + 1, \dots, L\}$. This leads to the first first-order condition

$$\frac{\partial \mathcal{L}}{\partial \mathbf{V}^{(\ell)}} = \sum_{n=1}^N \left\langle (\mathcal{X}_n - \mathcal{C} - \mathcal{U}_n \times \{\mathbf{V}\}) \odot \mathcal{W}_n, \mathcal{U}_n^{(-\ell)} \right\rangle_{\{L^*; L^*\}} = \mathbf{0}_{P_\ell \times K_\ell}.$$

The derivative of \mathcal{L} with respect to $u_{n,k_1\dots k_L}$ is

$$\begin{aligned}
\frac{\partial \mathcal{L}}{\partial u_{n,k_1\dots k_L}} &= \frac{\hat{\sigma}_2^2}{m} m_n \rho_2'(t_n/\hat{\sigma}_2) \frac{1}{\hat{\sigma}_2} \frac{\partial}{\partial u_{n,k_1\dots k_L}} \sqrt{\frac{1}{m_n} \sum_{p_1\dots p_L}^{P_1\dots P_L} m_{n,p_1\dots p_L} \hat{\sigma}_{1,p_1\dots p_L}^2 \rho_1\left(\frac{r_{n,p_1\dots p_L}}{\hat{\sigma}_{1,p_1\dots p_L}}\right)} \\
&= \frac{1}{2m} \frac{\psi_2(t_n/\hat{\sigma}_2)}{t_n/\hat{\sigma}_2} \frac{\partial}{\partial u_{n,k_1\dots k_L}} \left(\sum_{p_1\dots p_L}^{P_1\dots P_L} m_{n,p_1\dots p_L} \hat{\sigma}_{1,p_1\dots p_L}^2 \rho_1\left(\frac{r_{n,p_1\dots p_L}}{\hat{\sigma}_{1,p_1\dots p_L}}\right) \right) \\
&= \frac{1}{2m} \sum_{p_1\dots p_L}^{P_1\dots P_L} w_n^{case} \hat{\sigma}_{1,p_1\dots p_L}^2 \psi_1(r_{n,p_1\dots p_L}/\hat{\sigma}_{1,p_1\dots p_L}) \frac{m_{n,p_1\dots p_L}}{\hat{\sigma}_{1,p_1\dots p_L}} \frac{\partial r_{n,p_1\dots p_L}}{\partial u_{n,k_1\dots k_L}} \\
&= -\frac{1}{2m} \sum_{p_1\dots p_L}^{P_1\dots P_L} w_n^{case} \hat{\sigma}_{1,p_1\dots p_L} \frac{\psi_1(r_{n,p_1\dots p_L}/\hat{\sigma}_{1,p_1\dots p_L})}{r_{n,p_1\dots p_L}/\hat{\sigma}_{1,p_1\dots p_L}} \frac{m_{n,p_1\dots p_L}}{\hat{\sigma}_{1,p_1\dots p_L}} r_{n,p_1\dots p_L} v_{p_1 k_1}^{(1)} \cdots v_{p_L k_L}^{(L)} \\
&= -\frac{1}{2m} \sum_{p_1\dots p_L}^{P_1\dots P_L} w_n^{case} w_{n,p_1\dots p_L}^{cell} m_{n,p_1\dots p_L} r_{n,p_1\dots p_L} v_{p_1 k_1}^{(1)} \cdots v_{p_L k_L}^{(L)},
\end{aligned}$$

which results in the second first-order condition

$$\frac{\partial \mathcal{L}}{\partial \mathcal{U}_n} = ((\mathcal{X}_n - \mathcal{C} - \mathcal{U}_n \times \{\mathbf{V}\}) \odot \mathcal{W}_n) \times \{\mathbf{V}^T\} = \mathcal{O}_{K_1 \times \dots \times K_L}$$

The derivative of \mathcal{L} with respect to $c_{p_1\dots p_L}$ is

$$\begin{aligned}
\frac{\partial \mathcal{L}}{\partial c_{p_1\dots p_L}} &= \frac{\hat{\sigma}_2^2}{m} \sum_{n=1}^N m_n \rho_2'(t_n/\hat{\sigma}_2) \frac{1}{\hat{\sigma}_2} \frac{\partial}{\partial c_{p_1\dots p_L}} \sqrt{\frac{1}{m_n} \sum_{p_1\dots p_L}^{P_1\dots P_L} m_{n,p_1\dots p_L} \hat{\sigma}_{1,p_1\dots p_L}^2 \rho_1\left(\frac{r_{n,p_1\dots p_L}}{\hat{\sigma}_{1,p_1\dots p_L}}\right)} \\
&= \frac{1}{2m} \sum_{n=1}^N \frac{\psi_2(t_n/\hat{\sigma}_2)}{t_n/\hat{\sigma}_2} \frac{\partial}{\partial c_{p_1\dots p_L}} \left(\sum_{p_1\dots p_L}^{P_1\dots P_L} m_{n,p_1\dots p_L} \hat{\sigma}_{1,p_1\dots p_L}^2 \rho_1\left(\frac{r_{n,p_1\dots p_L}}{\hat{\sigma}_{1,p_1\dots p_L}}\right) \right) \\
&= \frac{1}{2m} \sum_{n=1}^N w_n^{case} \hat{\sigma}_{1,p_1\dots p_L}^2 \psi_1(r_{n,p_1\dots p_L}/\hat{\sigma}_{1,p_1\dots p_L}) \frac{m_{n,p_1\dots p_L}}{\hat{\sigma}_{1,p_1\dots p_L}} \frac{\partial}{\partial c_{p_1\dots p_L}} r_{n,p_1\dots p_L} \\
&= -\frac{1}{2m} \sum_{n=1}^N w_n^{case} \hat{\sigma}_{1,p_1\dots p_L} \frac{\psi_1(r_{n,p_1\dots p_L}/\hat{\sigma}_{1,p_1\dots p_L})}{r_{n,p_1\dots p_L}/\hat{\sigma}_{1,p_1\dots p_L}} \frac{m_{n,p_1\dots p_L}}{\hat{\sigma}_{1,p_1\dots p_L}} r_{n,p_1\dots p_L} \\
&= -\frac{1}{2m} \sum_{n=1}^N w_n^{case} w_{n,p_1\dots p_L}^{cell} m_{n,p_1\dots p_L} r_{n,p_1\dots p_L},
\end{aligned}$$

so the gradient with respect to the tensor \mathcal{C} becomes

$$\frac{\partial \mathcal{L}}{\partial \mathcal{C}} = \sum_{n=1}^N (\mathcal{X}_n - \mathcal{C} - \mathcal{U}_n \times \{\mathbf{V}\}) \odot \mathcal{W}_n = \mathcal{O}_{P_1 \times \dots \times P_L}.$$

In what follows, it is shown that the first order conditions of the ROMPCA objective function (4) are identical to those of the weighted MPCA objective function (13) given by

$$\begin{aligned}\tilde{\mathcal{L}}(\{\mathcal{X}_n\}, \{\mathbf{V}^{(\ell)}\}, \{\mathcal{U}_n\}, \mathcal{C}) &= \sum_{n=1}^N \sum_{p_1 \dots p_L}^{P_1 \dots P_L} w_{n,p_1 \dots p_L} \left(x_{n,p_1 \dots p_L} - c_{p_1 \dots p_L} - \sum_{k_1 \dots k_L}^{K_1 \dots K_L} u_{n,k_1 \dots k_L} v_{p_1 k_1}^{(1)} \dots v_{p_L k_L}^{(L)} \right)^2 \\ &= \sum_{n=1}^N \left\| \mathcal{W}_n^{1/2} \odot (\mathcal{X}_n - \mathcal{C} - \mathcal{U}_n \times \{\mathbf{V}\}) \right\|_F^2\end{aligned}\quad (\text{S.1})$$

The derivative of $\tilde{\mathcal{L}}$ with respect to $v_{p_\ell k_\ell}^{(\ell)}$ is

$$\begin{aligned}\frac{\partial \tilde{\mathcal{L}}}{\partial v_{p_\ell k_\ell}^{(\ell)}} &= \sum_{n=1}^N \frac{\partial}{\partial v_{p_\ell k_\ell}^{(\ell)}} \sum_{p_1 \dots p_L}^{P_1 \dots P_L} w_{n,p_1 \dots p_L} r_{n,p_1 \dots p_L}^2 \\ &= \frac{1}{2} \sum_{n=1}^N \sum_{p_\ell, \ell \in L^*} w_{n,p_1 \dots p_L} r_{n,p_1 \dots p_L} \frac{\partial r_{n,p_1 \dots p_L}}{\partial v_{p_\ell k_\ell}^{(\ell)}} \\ &= -\frac{1}{2} \sum_{n=1}^N \sum_{p_\ell, \ell \in L^*} \left[w_{n,p_1 \dots p_L} r_{n,p_1 \dots p_L} \sum_{k_\ell, \ell \in L^*} \left(u_{n,k_1 \dots k_L} v_{p_1 k_1}^{(1)} \dots v_{p_{\ell-1} k_{\ell-1}}^{(\ell-1)} v_{p_{\ell+1} k_{\ell+1}}^{(\ell+1)} \dots v_{p_L k_L}^{(L)} \right) \right]\end{aligned}$$

which results in

$$\frac{\partial \tilde{\mathcal{L}}}{\partial \mathbf{V}^{(\ell)}} = \sum_{n=1}^N \left\langle (\mathcal{X}_n - \mathcal{C} - \mathcal{U}_n \times \{\mathbf{V}\}) \odot \mathcal{W}_n, \mathcal{U}_n^{(-\ell)} \right\rangle_{\{L^*, L^*\}} = \mathbf{0}_{P_\ell \times K_\ell}$$

that is identical to (7). The derivative of $\tilde{\mathcal{L}}$ with respect to $u_{n,k_1 \dots k_L}$ is

$$\begin{aligned}\frac{\partial \tilde{\mathcal{L}}}{\partial u_{n,k_1 \dots k_L}} &= \frac{\partial}{\partial u_{n,k_1 \dots k_L}} \sum_{p_1 \dots p_L}^{P_1 \dots P_L} w_{n,p_1 \dots p_L} \left(x_{n,p_1 \dots p_L} - c_{p_1 \dots p_L} - \sum_{k_1 \dots k_L}^{K_1 \dots K_L} u_{n,k_1 \dots k_L} v_{p_1 k_1}^{(1)} \dots v_{p_L k_L}^{(L)} \right)^2 \\ &= \frac{1}{2} \sum_{p_1 \dots p_L}^{P_1 \dots P_L} w_{n,p_1 \dots p_L} r_{n,p_1 \dots p_L} \frac{\partial r_{n,p_1 \dots p_L}}{\partial u_{n,k_1 \dots k_L}} \\ &= -\frac{1}{2} \sum_{p_1 \dots p_L}^{P_1 \dots P_L} w_{n,p_1 \dots p_L} r_{n,p_1 \dots p_L} v_{p_1 k_1}^{(1)} \dots v_{p_L k_L}^{(L)},\end{aligned}$$

hence the second first-order condition is equal to (8):

$$\frac{\partial \tilde{\mathcal{L}}}{\partial \mathcal{U}_n} = ((\mathcal{X}_n - \mathcal{C} - \mathcal{U}_n \times \{\mathbf{V}\}) \odot \mathcal{W}_n) \times \{\mathbf{V}^T\} = \mathcal{O}_{K_1 \times \dots \times K_L}.$$

The derivative of $\tilde{\mathcal{L}}$ with respect to $c_{p_1 \dots p_L}$ is

$$\begin{aligned} \frac{\partial \tilde{\mathcal{L}}}{\partial c_{p_1 \dots p_L}} &= \sum_{n=1}^N w_{n,p_1 \dots p_L} \frac{\partial}{\partial c_{p_1 \dots p_L}} \left(x_{n,p_1 \dots p_L} - c_{p_1 \dots p_L} - \sum_{k_1 \dots k_L}^{K_1 \dots K_L} u_{n,k_1 \dots k_L} v_{p_1 k_1}^{(1)} \cdots v_{p_L k_L}^{(L)} \right)^2 \\ &= -\frac{1}{2} \sum_{n=1}^N w_{n,p_1 \dots p_L} r_{n,p_1 \dots p_L}, \end{aligned}$$

which results in condition (9):

$$\frac{\partial \tilde{\mathcal{L}}}{\partial \mathcal{C}} = \sum_{n=1}^N (\mathcal{X}_n - \mathcal{C} - \mathcal{U}_n \times \{\mathbf{V}\}) \odot \mathcal{W}_n = \mathcal{O}_{P_1 \times \dots \times P_L}.$$

B Description of the Algorithm

The IRLS starts with the initial estimates $\{\mathbf{V}_0^{(\ell)}\}$, $\{\mathcal{U}_{n,0}\}$ and \mathcal{C}_0 defined in Section 2.5, and the corresponding $\{\mathcal{W}_{n,0}\}$ obtained from (10), (11), (12), (5) and (6). Then, for each $q = 0, 1, 2, \dots$, new estimates $\{\mathbf{V}_{q+1}^{(\ell)}\}$, $\{\mathcal{U}_{n,q+1}\}$, \mathcal{C}_{q+1} and $\{\mathcal{W}_{n,q+1}\}$ are obtained from $\{\mathbf{V}_q^{(\ell)}\}$, $\{\mathcal{U}_{n,q}\}$, \mathcal{C}_q and $\{\mathcal{W}_{n,q}\}$ by the following procedure:

- (a) Minimize (13) with respect to $\mathbf{V}^{(\ell)}$ by substituting \mathcal{C}_q , $\{\tilde{\mathcal{U}}_{n,q}\}$, and $\{\mathcal{W}_{n,q}\}$ in (7). That is, for $\ell = 1, \dots, L$,

$$\begin{aligned} \sum_{n=1}^N \left\langle (\mathcal{X}_n - \mathcal{C}_q - \mathcal{U}_{n,q} \times \{\mathbf{V}\}) \odot \mathcal{W}_{n,q}, \mathcal{U}_{n,q}^{(-\ell)} \right\rangle_{\{L^*;L^*\}} &= \mathbf{0}_{P_\ell \times K_\ell}; \\ \sum_{n=1}^N \left\langle (\mathcal{U}_{n,q} \times \{\mathbf{V}\}) \odot \mathcal{W}_{n,q}, \mathcal{U}_{n,q}^{(-\ell)} \right\rangle_{\{L^*;L^*\}} &= \sum_{n=1}^N \left\langle (\mathcal{X}_n - \mathcal{C}_q) \odot \mathcal{W}_{n,q}, \mathcal{U}_{n,q}^{(-\ell)} \right\rangle_{\{L^*;L^*\}}; \\ \sum_{n=1}^N \left\langle (\mathcal{U}_{n,q}^{(-\ell)} \times_\ell \mathbf{V}^{(\ell)}) \odot \mathcal{W}_{n,q}, \mathcal{U}_{n,q}^{(-\ell)} \right\rangle_{\{L^*;L^*\}} &= \sum_{n=1}^N \left\langle (\mathcal{X}_n - \mathcal{C}_q) \odot \mathcal{W}_{n,q}, \mathcal{U}_{n,q}^{(-\ell)} \right\rangle_{\{L^*;L^*\}}, \end{aligned}$$

with $L^* = \{1, \dots, \ell - 1, \ell + 1, \dots, L\}$. Through unfolding, we have that

$$\begin{aligned} \sum_{n=1}^N \left\langle (\mathbf{V}^{(\ell)} \mathbf{U}_{n(\ell),q}^{(-\ell)}) \odot \mathbf{W}_{n(\ell),q}, \mathbf{U}_{n(\ell),q}^{(-\ell)} \right\rangle_{\{L^*;L^*\}} &= \sum_{n=1}^N \left\langle (\mathbf{X}_{n(\ell)} - \mathbf{C}_{(\ell),q}) \odot \mathbf{W}_{n(\ell),q}, \mathbf{U}_{n(\ell),q}^{(-\ell)} \right\rangle_{\{L^*;L^*\}} \\ \sum_{n=1}^N \left((\mathbf{V}^{(\ell)} \mathbf{U}_{n(\ell),q}^{(-\ell)}) \odot \mathbf{W}_{n(\ell),q} \right) \mathbf{U}_{n(\ell),q}^{(-\ell)T} &= \sum_{n=1}^N ((\mathbf{X}_{n(\ell)} - \mathbf{C}_{(\ell),q}) \odot \mathbf{W}_{n(\ell),q}) \mathbf{U}_{n(\ell),q}^{(-\ell)T}. \end{aligned}$$

By vectorizing this last equation, we have that

$$\begin{aligned}
& \sum_{n=1}^N \left(\mathbf{U}_{n(\ell),q}^{(-\ell)} \otimes \mathbf{I}_{P_\ell} \right) \left(\text{vec} \left(\mathbf{V}^{(\ell)} \mathbf{U}_{n(\ell),q}^{(-\ell)} \right) \odot \text{vec} \left(\mathbf{W}_{n(\ell),q} \right) \right) \\
& \quad = \sum_{n=1}^N \left(\mathbf{U}_{n(\ell),q}^{(-\ell)} \otimes \mathbf{I}_{P_\ell} \right) \left(\text{vec} \left(\mathbf{X}_{n(\ell)} - \mathbf{C}_{(\ell),q} \right) \odot \text{vec} \left(\mathbf{W}_{n(\ell),q} \right) \right); \\
& \sum_{n=1}^N \left(\mathbf{U}_{n(\ell),q}^{(-\ell)} \otimes \mathbf{I}_{P_\ell} \right) \mathbf{W}_{n,q} \text{vec} \left(\mathbf{V}^{(\ell)} \mathbf{U}_{n(\ell),q}^{(-\ell)} \right) \\
& \quad = \sum_{n=1}^N \left(\mathbf{U}_{n(\ell),q}^{(-\ell)} \otimes \mathbf{I}_{P_\ell} \right) \mathbf{W}_{n,q} \text{vec} \left(\mathbf{X}_{n(\ell)} - \mathbf{C}_{(\ell),q} \right); \\
& \left[\sum_{n=1}^N \left(\mathbf{U}_{n(\ell),q}^{(-\ell)} \otimes \mathbf{I}_{P_\ell} \right) \mathbf{W}_{n,q} \left(\mathbf{U}_{n(\ell),q}^{(-\ell)} \otimes \mathbf{I}_{P_\ell} \right)^T \right] \text{vec} \left(\mathbf{V}^{(\ell)} \right) \\
& \quad = \sum_{n=1}^N \left(\mathbf{U}_{n(\ell),q}^{(-\ell)} \otimes \mathbf{I}_{P_\ell} \right) \mathbf{W}_{n,q} \text{vec} \left(\mathbf{X}_{n(\ell)} - \mathbf{C}_{(\ell),q} \right).
\end{aligned}$$

Thus,

$$\text{vec} \left(\mathbf{V}_{q+1}^{(\ell)} \right) = \left[\sum_{n=1}^N \left(\mathbf{U}_{n(\ell),q}^{(-\ell)} \otimes \mathbf{I}_{P_\ell} \right) \mathbf{W}_{n,q} \left(\mathbf{U}_{n(\ell),q}^{(-\ell)} \otimes \mathbf{I}_{P_\ell} \right)^T \right]^\dagger \left[\sum_{n=1}^N \left(\mathbf{U}_{n(\ell),q}^{(-\ell)} \otimes \mathbf{I}_{P_\ell} \right) \mathbf{W}_{n,q} \text{vec} \left(\mathbf{X}_{n(\ell)} - \mathbf{C}_{(\ell),q} \right) \right].$$

where \dagger denotes the Moore-Penrose generalized inverse. Here the use of the generalized inverse is justified by the fact that $\sum_{n=1}^N (\mathbf{U}_{n(\ell),q}^{(-\ell)} \otimes \mathbf{I}_{P_\ell}) \mathbf{W}_{n,q} (\mathbf{U}_{n(\ell),q}^{(-\ell)} \otimes \mathbf{I}_{P_\ell})^T$ can be singular, e.g, when the weight matrices $\mathbf{W}_{n,q}$ have too many zeros.

- (b) Minimize (13) with respect to \mathcal{U}_n by substituting $\{\mathbf{V}_{q+1}^{(\ell)}\}$, \mathcal{C}_q , and $\{\mathcal{W}_{n,q}\}$ in (8). That is, for $n = 1, \dots, N$,

$$\left((\mathcal{X}_n - \mathcal{C}_q - \mathcal{U}_n \times \{\mathbf{V}_{q+1}\}) \odot \mathcal{W}_{n,q} \right) \times \{\mathbf{V}_{q+1}^T\} = \mathcal{O}_{K_1 \times \dots \times K_L}. \quad (\text{S.2})$$

Instead we solve

$$\left((\mathcal{X}_n - \mathcal{C}_q - \mathcal{U}_n \times \{\mathbf{V}_{q+1}\}) \odot \widetilde{\mathcal{W}}_{n,q} \right) \times \{\mathbf{V}_{q+1}^T\} = \mathcal{O}_{K_1 \times \dots \times K_L} \quad (\text{S.3})$$

with $\widetilde{\mathcal{W}}_{n,q} = \mathcal{W}_{n,q}^{\text{cell}} \odot \mathcal{M}_n$. This is justified since (S.2) is equivalent to (S.3) when $w_n^{\text{case}} \neq 0$. For a tensor with $w_n^{\text{case}} = 0$, the term $\left\| \mathcal{W}_n^{1/2} \odot (\mathcal{X}_n - \mathcal{C} - \mathcal{U}_n \times \{\mathbf{V}\}) \right\|_F^2$ in (S.1) is minimal as it is zero. Then

$$\left((\mathcal{U}_n \times \{\mathbf{V}_{q+1}\}) \odot \widetilde{\mathcal{W}}_{n,q} \right) \times \{\mathbf{V}_{q+1}^T\} = \left((\mathcal{X}_n - \mathcal{C}_q) \odot \widetilde{\mathcal{W}}_{n,q} \right) \times \{\mathbf{V}_{q+1}^T\}.$$

By vectorizing this last equation, we have that

$$\begin{aligned} \left(\bigotimes_{\ell=1}^L \mathbf{V}_{q+1}^{(\ell)T} \right) \left(\text{vec} (\mathcal{U}_n \times \{\mathbf{V}_{q+1}\}) \odot \text{vec} (\widetilde{\mathcal{W}}_{n,q}) \right) &= \left(\bigotimes_{\ell=1}^L \mathbf{V}_{q+1}^{(\ell)T} \right) \left(\text{vec} (\mathcal{X}_n - \mathcal{C}_q) \odot \text{vec} (\widetilde{\mathcal{W}}_{n,q}) \right); \\ \left(\bigotimes_{\ell=1}^L \mathbf{V}_{q+1}^{(\ell)T} \right) \widetilde{\mathcal{W}}_{n,q} \left(\bigotimes_{\ell=1}^L \mathbf{V}_{q+1}^{(\ell)} \right) \text{vec} (\mathcal{U}_n) &= \left(\bigotimes_{\ell=1}^L \mathbf{V}_{q+1}^{(\ell)T} \right) \widetilde{\mathcal{W}}_{n,q} \text{vec} (\mathcal{X}_n - \mathcal{C}_q). \end{aligned}$$

Thus,

$$\text{vec} (\mathcal{U}_{n,q+1}) = \left[\left(\bigotimes_{\ell=1}^L \mathbf{V}_{q+1}^{(\ell)T} \right) \widetilde{\mathcal{W}}_{n,q} \left(\bigotimes_{\ell=1}^L \mathbf{V}_{q+1}^{(\ell)} \right) \right]^\dagger \left[\left(\bigotimes_{\ell=1}^L \mathbf{V}_{q+1}^{(\ell)T} \right) \widetilde{\mathcal{W}}_{n,q} \text{vec} (\mathcal{X}_n - \mathcal{C}_q) \right].$$

(c) Minimize (13) with respect to \mathcal{C} by substituting $\{\mathbf{V}_{q+1}^{(\ell)}\}$, $\{\mathcal{U}_{n,q+1}\}$, and $\{\mathcal{W}_{n,q}\}$ in (9). That is

$$\begin{aligned} \sum_{n=1}^N (\mathcal{X}_n - \mathcal{U}_{n,q+1} \times \{\mathbf{V}_{q+1}\} - \mathcal{C}) \odot \mathcal{W}_{n,q} &= \mathcal{O}_{P_1 \times \dots \times P_L} \\ \mathcal{C} \odot \left(\sum_{n=1}^N \mathcal{W}_{n,q} \right) &= \sum_{n=1}^N (\mathcal{X}_n - \mathcal{U}_{n,q+1} \times \{\mathbf{V}_{q+1}\}) \odot \mathcal{W}_{n,q}. \end{aligned}$$

Thus,

$$\mathcal{C}_{q+1} = \left(\sum_{n=1}^N (\mathcal{X}_n - \mathcal{U}_{n,q+1} \times \{\mathbf{V}_{q+1}\}) \odot \mathcal{W}_{n,q} \right) \odot \mathcal{H}_q.$$

(d) Update $\{\mathcal{W}_{n,q}\}$ using (10), (11), (12), (5) and (6) with $\{\mathbf{V}_{q+1}^{(\ell)}\}$, $\{\mathcal{U}_{n,q+1}\}$, and \mathcal{C}_{q+1} .

C Proof of Proposition 1

In this section Proposition 1 is proved, which ensures that each step of the algorithm decreases the objective function (4).

The proof of Proposition 1 follows the steps of Centofanti et al. (2024) and is based on the following lemmas.

Lemma 1. For given weight tensors $\{\mathcal{W}_{n,q}\}$, each of the update steps (a), (b), and (c) of the algorithm in Section B decrease the weighted MPCA objective function (13).

Lemma 2. The function $\mathbf{f} \rightarrow L(\mathbf{f})$ is concave.

Proof. It is shown in Centofanti et al. (2024) that the univariate function $h : \mathbb{R}_+ \rightarrow \mathbb{R}_+ : z \rightarrow \rho_{b,c}(\sqrt{z})$, in which $\rho_{b,c}$ is the hyperbolic tangent ρ -function, is concave.

By the definition of concavity of a multivariate function, we need to prove that for any column vectors $\mathbf{f}^1, \mathbf{f}^2$ in \mathbb{R}_+^D and any λ in $(0, 1)$ it holds that $L(\lambda \mathbf{f}^1 + (1 - \lambda) \mathbf{f}^2) \geq \lambda L(\mathbf{f}^1) + (1 - \lambda) L(\mathbf{f}^2)$.

This follows from

$$\begin{aligned}
L(\lambda \mathbf{f}^1 + (1 - \lambda) \mathbf{f}^2) &= \frac{\hat{\sigma}_2^2}{m} \sum_{n=1}^N h_2 \left(\frac{1}{m_n \hat{\sigma}_2^2} \sum_{p_1 \dots p_L}^{P_1 \dots P_L} m_{n, p_1 \dots p_L} \hat{\sigma}_{1, p_1 \dots p_L}^2 h_1 \left(\frac{\lambda f_{d_n, p_1 \dots p_L}^1 + (1 - \lambda) f_{d_n, p_1 \dots p_L}^2}{\hat{\sigma}_{1, p_1 \dots p_L}^2} \right) \right) \\
&\geq \frac{\hat{\sigma}_2^2}{m} \sum_{n=1}^N h_2 \left(\frac{1}{m_n \hat{\sigma}_2^2} \sum_{p_1 \dots p_L}^{P_1 \dots P_L} m_{n, p_1 \dots p_L} \hat{\sigma}_{1, p_1 \dots p_L}^2 \left[\lambda h_1 \left(\frac{f_{d_n, p_1 \dots p_L}^1}{\hat{\sigma}_{1, p_1 \dots p_L}^2} \right) \right. \right. \\
&\qquad \qquad \left. \left. + (1 - \lambda) h_1 \left(\frac{f_{d_n, p_1 \dots p_L}^2}{\hat{\sigma}_{1, p_1 \dots p_L}^2} \right) \right] \right) \\
&= \frac{\hat{\sigma}_2^2}{m} \sum_{n=1}^N h_2 \left(\lambda \frac{1}{m_n \hat{\sigma}_2^2} \sum_{p_1 \dots p_L}^{P_1 \dots P_L} m_{n, p_1 \dots p_L} \hat{\sigma}_{1, p_1 \dots p_L}^2 h_1 \left(\frac{f_{d_n, p_1 \dots p_L}^1}{\hat{\sigma}_{1, p_1 \dots p_L}^2} \right) \right. \\
&\qquad \qquad \left. + (1 - \lambda) \frac{1}{m_n \hat{\sigma}_2^2} \sum_{p_1 \dots p_L}^{P_1 \dots P_L} m_{n, p_1 \dots p_L} \hat{\sigma}_{1, p_1 \dots p_L}^2 h_1 \left(\frac{f_{d_n, p_1 \dots p_L}^2}{\hat{\sigma}_{1, p_1 \dots p_L}^2} \right) \right) \\
&\geq \frac{\hat{\sigma}_2^2}{m} \sum_{n=1}^N \left[\lambda h_2 \left(\frac{1}{m_n \hat{\sigma}_2^2} \sum_{p_1 \dots p_L}^{P_1 \dots P_L} m_{n, p_1 \dots p_L} \hat{\sigma}_{1, p_1 \dots p_L}^2 h_1 \left(\frac{f_{d_n, p_1 \dots p_L}^1}{\hat{\sigma}_{1, p_1 \dots p_L}^2} \right) \right) \right. \\
&\qquad \qquad \left. + (1 - \lambda) h_2 \left(\frac{1}{m_n \hat{\sigma}_2^2} \sum_{p_1 \dots p_L}^{P_1 \dots P_L} m_{n, p_1 \dots p_L} \hat{\sigma}_{1, p_1 \dots p_L}^2 h_1 \left(\frac{f_{d_n, p_1 \dots p_L}^2}{\hat{\sigma}_{1, p_1 \dots p_L}^2} \right) \right) \right] \\
&= \lambda L(\mathbf{f}^1) + (1 - \lambda) L(\mathbf{f}^2).
\end{aligned}$$

The first inequality follows from the concavity of h_1 and the fact that h_2 is nondecreasing. The second inequality comes from the concavity of h_2 . Thus, L is a concave function. \square

The weighted MPCA objective (13) can also be written as a function of \mathbf{f} . Denote it as $L_{\mathbf{w}}(\mathbf{f}) := \mathbf{w}^T \mathbf{f}$, where $\mathbf{w} = \{\text{vec}(\mathcal{W}_n)\}_{n=1}^N$ turns the weight tensors into a vector in the same way as the column vector \mathbf{f} . Lemma 3 links the weighted MPCA objective $L_{\mathbf{w}}$ with the original objective L .

Lemma 3. If two column vectors $\mathbf{f}^1, \mathbf{f}^2 \in \mathbb{R}_+^D$ satisfy $L_{\mathbf{w}}(\mathbf{f}^1) \leq L_{\mathbf{w}}(\mathbf{f}^2)$, then $L(\mathbf{f}^1) \leq L(\mathbf{f}^2)$.

Proof. By using Lemma 2 and Centofanti et al. (2024).

Proof of Proposition 1. When the fit is updated from $\boldsymbol{\theta}_q$ to $\boldsymbol{\theta}_{q+1}$, Lemma 1 shows that $L_{\mathbf{w}_q}(\mathbf{f}(\boldsymbol{\theta}_{q+1})) \leq L_{\mathbf{w}_q}(\mathbf{f}(\boldsymbol{\theta}_q))$, so using Lemma 3 it follows that $L(\mathbf{f}(\boldsymbol{\theta}_{q+1})) \leq L(\mathbf{f}(\boldsymbol{\theta}_q))$. \square

D The Rank Determination Method

To illustrate the performance of the rank determination method proposed in Section 2.7, we consider a data set generated as in Section 3 with $(P_1, P_2, P_3) = (15, 10, 5)$ and $(K_1, K_2, K_3) = (4, 3, 2)$. The cumulative eigenvalues obtained from $\{\mathcal{X}_n\}$ are plotted in the left panel of Figure S.1. We clearly see that the cumulative variance in each mode stabilizes at the corresponding dimensions of the core tensor.

Next we contaminate the data with cellwise and casewise outliers according to the procedure outlined in Section 2.7, with $\gamma_{cell} = 5$. The cumulative eigenvalues derived from $\{\mathcal{X}_h^{DDC}\}$ are shown in the right panel of Figure S.1 and are almost identical to the those of the left panel. This illustrates the effectiveness of our proposed rank determination method.

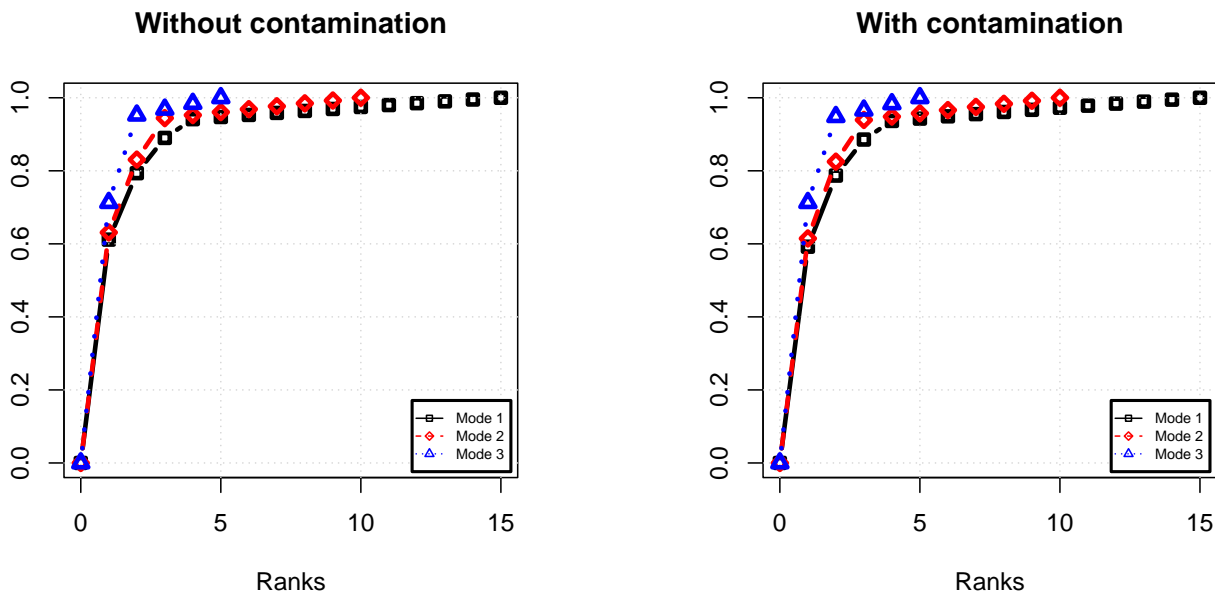


Figure S.1: Cumulative eigenvalues at an uncontaminated data set (left) and at a contaminated data set (right).

E Additional Simulation Results

Here, we provide the results for the lower dimensional setting for $(P_1, P_2, P_3) = (15, 10, 5)$ and $(K_1, K_2, K_3) = (4, 3, 2)$. Figures S.2 and S.3 show the median MSE for the three contamination scenarios in absence and presence of missing values, respectively. The resulting curves are very similar to the results in Section 3 of the paper, leading to the same conclusions.

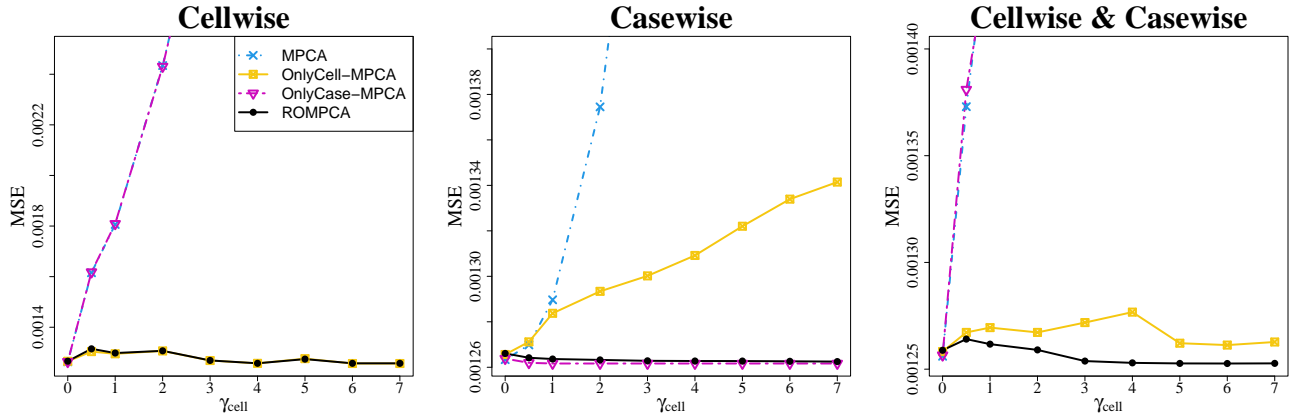


Figure S.2: Median MSE attained by MPCA, OnlyCase-MPCA, OnlyCell-MPCA, and ROMPCA for the setting $(P_1, P_2, P_3) = (15, 10, 5)$ and $(K_1, K_2, K_3) = (4, 3, 2)$ under cellwise contamination, casewise contamination or both, in function of γ_{cell} for data without missing values.

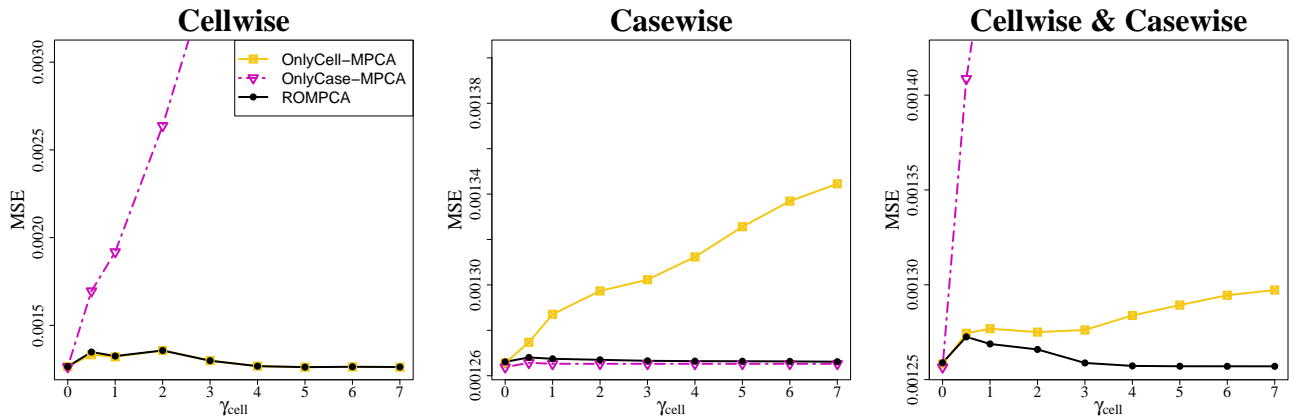


Figure S.3: Median MSE attained by OnlyCase-MPCA, OnlyCell-MPCA, and ROMPCA for the setting $(P_1, P_2, P_3) = (15, 10, 5)$ and $(K_1, K_2, K_3) = (4, 3, 2)$ under cellwise contamination, casewise contamination or both, in function of γ_{cell} for data with 10% of missing values.

F Additional Results for the Dog Walker Data

To reduce the dimensionality of the Dog Walker data, the rank of the projection matrices must first be determined. The ranks for ROMPCA are identified as (1, 1, 1) based on the plot of the cumulative eigenvalues for each mode in the left frame of Figure S.4. The ranks (1, 1, 1) suggest that the center already explains a large portion of the data variability. However, additional variability remains, which is captured in the core tensors $\{\mathcal{U}_n\}$. As shown in Figure 11 the set of core tensors reveal a non-constant pattern. This indicates the presence of variability that cannot be fully explained using only the center.

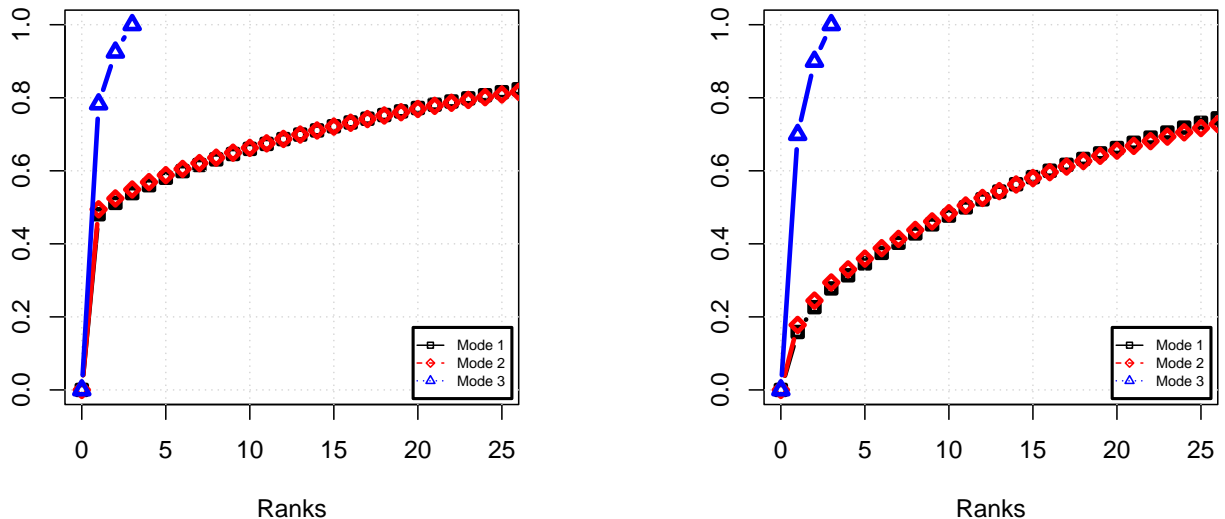


Figure S.4: Comparison of the cumulative eigenvalues for the Dog Walker data using ROMPCA (left) and MPCA (right).

The right frame of Figure S.4 shows the cumulative eigenvalues of MPCA. We choose the ranks as (9, 9, 1) to match the variance explained from the robust procedure, and apply MPCA. Figure S.5 compares some of the original frames with the reconstructed frames from MPCA. We clearly see that the background is not well separated from the walking man.

The dog walker example allows us to illustrate the added value of using a multilinear approach. Figure S.6 shows two residual cellmaps using 100 aggregated columns. The top panel is the residual cellmap obtained from DDC applied to the vectorized frames, while the bottom panel is the ROMPCA residual cellmap. In contrast to ROMPCA, the multivariate DDC method flags nearly all cells in the first frames as outliers. It is thus not able to capture the variation in the illumination.



Figure S.5: Frames from the Dog Walker data (upper row) and reconstructed data frames using MPCA (lower row).

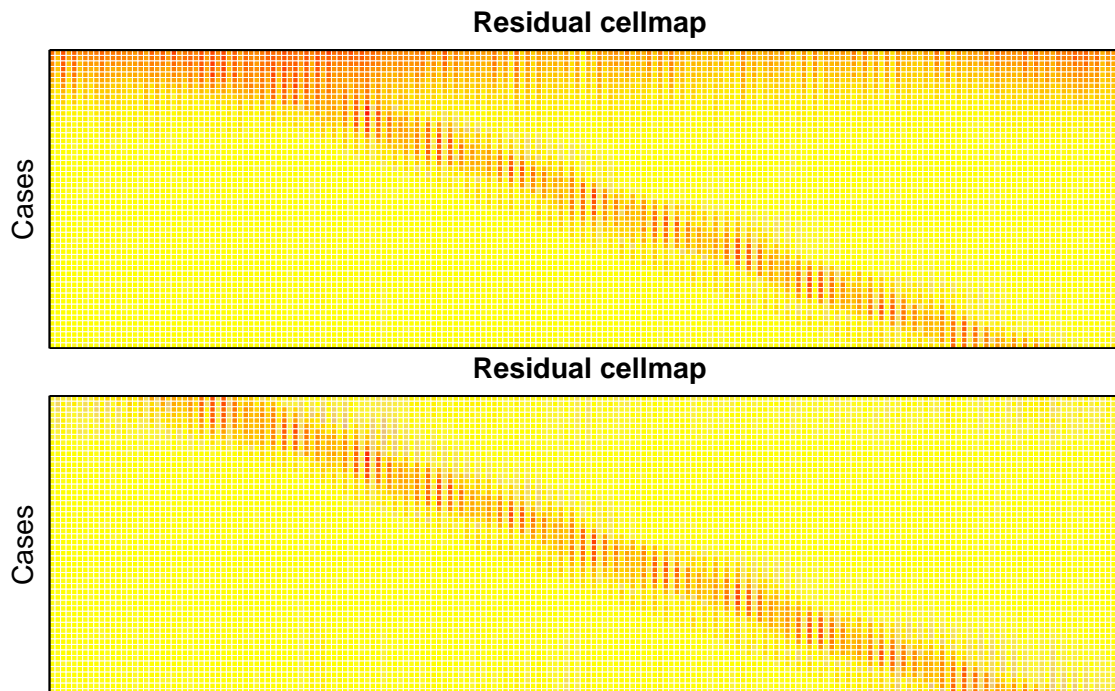


Figure S.6: Residual cellmap from DDC (top) and ROMPCA (bottom).

G Additional Results for the Dorrit Data

Applying the elbow rule to the plot of the cumulative eigenvalues in Figure S.7 suggests to set the ranks to $(K_1, K_2) = (4, 4)$. This is in line with the ranks used in Goldfarb and Qin (2014) in their data application for the Dorrit data.

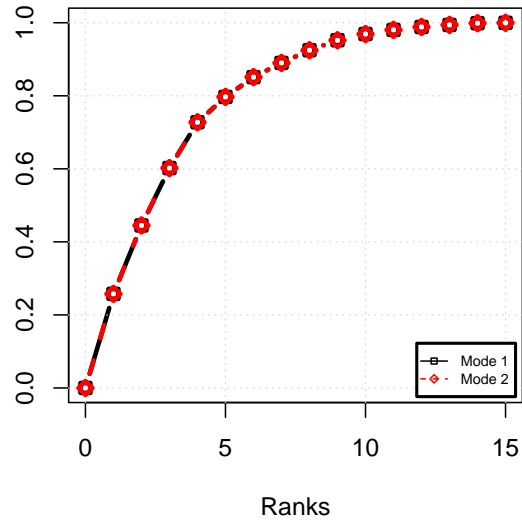


Figure S.7: Cumulative eigenvalues using DDC imputation on the Dorrit data.